Learning from the past: Impact of the Arctic Oscillation on sea ice and marine productivity off northwest Greenland over the last 9,000 years

Audrey Limoges, Kaarina Weckström, Sofia Ribeiro, Eleanor Georgiadis, Katrine Elnegaard Hansen, Philippe Martinez, Marit-Solveig Seidenkrantz, Jacques Giraudeau, Xavier Crosta, Guillaume Massé

DR. AUDREY LIMOGES (Orcid ID : 0000-0002-4587-3417)
DR. KAARINA WECKSTRÖM (Orcid ID : 0000-0002-3889-0788)

Article type : Primary Research Articles

Learning from the past: impact of the Arctic Oscillation on sea ice and marine productivity off northwest Greenland over the last 9000 years

Audrey Limoges[1*], Kaarina Weckström[2], Sofia Ribeiro[3], Eleanor Georgiadis[4], Katrine Elnegaard Hansen[5], Philippe Martinez[4], Marit-Solveig Seidenkrantz[5], Jacques Giraudeau[4], Xavier Crosta[4], Guillaume Massé[6,7]

[1] Department of Earth Sciences, University of New Brunswick, Fredericton, Canada,
[2] Ecosystems and Environment Research Programme (ECRU), and Helsinki Institute of Sustainability Science, Helsinki University, Finland
[3] Department of Glaciology and Climate, Geological Survey of Denmark and Greenland, Copenhagen, Denmark
[4] Université de Bordeaux, CNRS, EPHE, UMR 5805 EPOC, Pessac, France
[5] Department of Geosciences, Aarhus University, Aarhus, Denmark
[6] Université Laval, CNRS, UMI 3376 TAKUVIK, Québec, Canada
[7] Station Marine de Concarneau, UMR7159 LOCEAN, Concarneau, France

***Correspondence**
Audrey Limoges, Department of Earth Sciences, University of New Brunswick, 2 Bailey Drive, Fredericton, New Brunswick, E3B 5A3, Canada.
Email: alimoges@unb.ca

ABSTRACT

Climate warming is rapidly reshaping the Arctic cryosphere and ocean conditions, with consequences for sea ice and pelagic productivity patterns affecting the entire marine food web. To predict how ongoing changes will impact Arctic marine ecosystems, concerted effort from various disciplines is required. Here, we contribute multi-decadal reconstructions of changes in diatom production and sea-ice conditions in relation to Holocene climate and ocean conditions off Northwest Greenland. Our multiproxy study includes diatoms, sea-ice biomarkers (IP_{25} and HBI III) and geochemical tracers (TOC, TOC:TN, $\delta^{13}C$, $\delta^{15}N$) from a sediment core record spanning the last ca. 9000 years. Our results suggest that the balance between the outflow of polar water from the Arctic, and input of Atlantic water from the Irminger Current into the West Greenland Current is a key factor in controlling sea-ice conditions, and both diatom phenology and production in northeastern Baffin Bay. Our proxy record notably shows that changes in sea-surface conditions initially forced by Neoglacial cooling were dynamically amplified by the shift in the dominant phase of the Arctic Oscillation (AO) mode that occurred at ca. 3000 yrs BP, and caused drastic changes in community composition and a decline in diatom production at the study site. In the future, with projected dominant positive AO conditions favored by Arctic warming, increased water column stratification may counteract the positive effect of a longer open-water growth season and negatively impact diatom production.

KEYWORDS

climate change, Baffin Bay, Arctic Oscillation, paleoceanography, phytoplankton, marine sediment, highly branched isoprenoid (HBI) biomarkers, diatoms

1. Introduction

Climate change is causing an accelerating decline in the seasonal duration and thickness of Arctic sea ice (Serreze and Stroeve, 2015), with important implications for marine primary production (e.g.,

Comeau *et al*. 2011; Tremblay *et al*. 2012; Bergeron and Tremblay 2014). For the Arctic Ocean, satellite-based measurements suggest that annual net primary production has increased by 30% between 1998 and 2012 (Arrigo and van Dijken 2015). This increase is largely attributed to thinning sea ice and more abundant and larger melt ponds that allow greater light transmittance and earlier onset of seasonal sea-ice melt, thereby enhancing both the under-ice productivity and the length of the growing season (Arrigo *et al*. 2012; Mundy *et al*. 2009). However, both satellite observations and *in situ* measurements indicate pronounced spatial and interannual heterogeneity in the response of primary producers to ongoing Arctic warming owing to local and remote factors that can have a synergistic impact on nutrient supplies and sea-surface conditions (e.g., ocean currents, vertical mixing, upstream biological processes) (e.g., Tremblay *et al*. 2015; Hopwood *et al.* 2018). Determining future changes in Arctic primary production in a scenario of continued climate warming is therefore challenging, especially since our understanding of how primary production responded to climate forcing on longer time scales is limited by the paucity of comprehensive and highly resolved paleoarchives.

In addition to radiative forcing, variability in hemispheric-scale atmospheric circulation patterns can impact ecosystem functioning (Post and Forchlammer 2002). The Arctic Oscillation (AO), also referred to as the Northern Annular Mode (NAM), is described as the difference in sea-level pressure between the Arctic Ocean and the middle latitudes (Thompson and Wallace 1998; Rigor *et al*. 2002; Cohen and Barlow 2005). The region defined for AO overlaps with the closely related North Atlantic Oscillation (NAO), which measures the regional variability in the atmospheric high- and low-pressure systems over the Azores and Iceland, respectively (Wallace 2000). Instrumental time series capture a dynamic relationship between the AO and interannual variations in storminess, sea-surface temperatures and sea-ice motion and conditions (e.g., Rodwell et al. 1999; Thompson and Wallace 2001; Ogi and Wallace 2007; Zweng and Münchow 2006; Weckström *et al.* 2013). During a positive phase, lower-than-normal pressure over the Arctic traps cold air masses in the Arctic, but wintertime surface winds and thermodynamic processes can lead to an overall thinning of the sea-ice cover over the Arctic Ocean. Therefore, although positive winter AO is associated with a cold anomaly in the surface atmospheric temperature over the Arctic Ocean and Greenland, it counterintuitively results in

an earlier Arctic Ocean ice melt and increased export of meltwater and drift ice via the Transpolar Drift through Fram Strait (Rigor *et al*. 2002) and other gateways such as Nares Strait (Figure 1b). In the northern North Atlantic sector, a positive phase correlates with cold west Greenlandic winters caused by a strengthening of the Baffin Bay and North Atlantic westerlies (Box 2002). Inversely, negative AO facilitates the buildup of multiyear ice in a strong Beaufort Gyre (Rigor *et al*. 2002), is associated with reduced export of Arctic freshwater and sea ice via the Arctic gateways, and the prevalence of milder atmospheric winter temperatures along the west Greenland margin. AO can swing between its high and low index polarity within weeks, but persistent modes can also be sustained on decadal to millennial timescales (e.g., Funder *et al.* 2011; Darby *et al*. 2012; Olsen *et al.* 2012). On the Holocene timescale, studies suggest linkages between hemispheric atmospheric circulation and hydrographical conditions in the North Atlantic region (e.g., Andersen et *al.* 2004; Solignac *et al.* 2004; Giraudeau *et al.* 2010; Moros e*t al.* 2012; Staines-Urías *et al.* 2013; Van Nieuwenhove *et al.* 2018), and along the Southeast and Western Greenland shelves (e.g., Jennings *et al.* 2011; Sha *et al*. 2011; Krawczyk *et al.* 2013).

In northern Baffin Bay, oceanographic conditions are influenced by incursions of cold, silica- and phosphate-rich water originating partly from the Pacific and entering Baffin Bay via Nares Strait, Lancaster Sound and Jones Sound (Figure 1), and the northward-flowing West Greenland Current (WGC) (200-700m) (Straneo 2006), which is overlain by buoyant meltwater and iceberg supplies from the Greenland Ice Sheet. The WGC is composed of a mixture of cold and low-salinity polar water carried by the East Greenland Current (EGC), an extension of the Transpolar Drift, and temperate, salty and nitrate-rich water derived from the Irminger Current (>3.5°C, >34.88 psu; Myers *et al*. 2007), a branch of the North Atlantic Current (Figure 1b). During intervals of increased export of freshwater and drift ice through Fram Strait, such as during contemporary high index polarity of the AO, a stronger EGC can contribute to a longitudinal expansion of the North Atlantic subpolar gyre, and reduce the northwestward flow of the warm Irminger Water into the WGC (e.g., Flatau *et al*. 2003; Sarafanov 2009; Morley *et al*. 2014). By contrast, a weaker EGC can be associated with a contracted subpolar gyre and increased northwestward flow of warm Irminger Water into the WGC (e.g., Holland *et al.* 2008; Jennings *et al.* 2011). Thus, the dominant mode of atmospheric circulation

can indirectly influence the strength and heat advected by the WGC, and amplify changes in surface-water properties and ocean-ice sheet interactions along the West Greenland margin. At the same time, the AO polarity index influences the consolidation or collapse of the ice arches in Nares Strait (e.g., Georgiadis *et al.* 2020), thereby also modulating the outflow of Arctic freshwater and drift ice through this gateway.

Given the key role of northern Baffin Bay as mediator between the Arctic and North Atlantic oceans, a number of studies documenting changes in regional ocean conditions in relation to Holocene climate fluctuations have been conducted (e.g., Levac *et al.* 2001; Mudie *et al*. 2005; Knudsen *et al.* 2008; St-Onge and St-Onge, 2014; Caron *et al.* 2018, 2019; Hansen *et al.* 2020; Saini *et al.* 2020; Giraudeau *et al.* 2020). However, the link between atmosphere-ocean forcing as expressed by swings in the dominant mode of the AO and changes in sea-ice seasonality and primary production in northern Baffin Bay has never been investigated. Here, we examine long-term changes in sea ice and primary production off Northwest Greenland, northeastern Baffin Bay, using a series of biogenic proxies applied to a 7.34 m-long sediment core spanning the last ca. 9000 years. We also provide a continuous and high-resolution record of changes in diatom production and sea-ice conditions which can serve as a reference baseline to interpret recent changes and better predict the response of primary producers to future climate change.

2. Material and Methods

The marine sediment core AMD14-204 was collected using a Calypso Square gravity corer, in the cross-shelf trough north of the Upernavik Ice Stream (73°15.66'N–57°53.98'W, 987m water depth) (Figure 1C), during the 2014 ArcticNet Leg 1b onboard the CCGS *Amundsen*. The core was subsampled onboard using u-channels and stored at 4°C during transportation. Subsamples for biomarker analyses were stored at -80°C until analysis. Detailed core lithology information is available in Caron *et al.* (2018).

3.1 Age model

The core chronology is based on 11 accelerator mass spectrometry ^{14}C dates from 15 samples of planktic and mixed benthic foraminiferal assemblages, a few also including ostracods (Table 1, Figure 2) (Hansen *et al*. 2020). All dates were calibrated using the Marine13 radiocarbon calibration curve (Reimer *et al.* 2013) and an additional reservoir age correction (ΔR) of 140 +/- 30 years was applied (Lloyd *et al.* 2011). For the age depth modelling, a depositional P_sequence model was used with a k-value of 0.68 (Ramsey 2008). Based on this age model, the core spans the last 9.2 cal kyrs BP (hereafter simply expressed as kyrs BP).

3.2 Sedimentary proxies

3.2.1 Total organic carbon and nitrogen isotopic analysis

Sedimentary organic carbon is derived from biomass decomposition and can include organic carbon of terrestrial and marine origins. For the total organic carbon (TOC) analyses, the inorganic carbon fraction was removed by adding hydrochloric acid (HCl, 10%) to freeze-dried samples. HCl was evaporated by heating the samples for 12 hours, TOC was then measured with a LECO C-S 125 analyser.

Assuming that diagenetic enrichment (Robinson *et al.* 2012) of ^{15}N is constant through time, the nitrogen isotopic ($\delta^{15}N$) signal in marine sediments reflects nitrate (NO_3^-) supply and use in the euphotic zone. Light nitrate ($^{14}NO_3^-$) is preferentially used by phytoplankton, resulting in higher $\delta^{15}N$ values when phytoplankton production is elevated. Alternatively, a change in the nitrate inventory of the water masses, linked to changes in nutrient supplies, stratification of the water column or ocean circulation can also alter the sedimentary $\delta^{15}N$ signal. At constant primary production rates, higher input of nitrate to the surface water can result in lower $\delta^{15}N$ values. Additionally, the organic matter TOC:TN ratio and $\delta^{13}C$ can be used to discriminate between terrestrial, sympagic and marine sources of sedimentary organic matter. For isotopic measurements of carbon, samples were treated with HCl followed by two distilled water rinses and were oven-dried prior to measurements with an IRMS (IsoPrime GV). Nitrogen content and isotopic ratios were measured on untreated freeze-dried samples

with an Elemental Analyser (Flash2000, ThermoFisher) coupled with the IRMS (S1). Carbon and nitrogen analyses were conducted at a 5 to 20 cm sampling interval, which corresponds to an effective age resolution of ca. 75 to 440 yrs (mean: ~175 yrs).

3.2.2 Diatoms

Diatoms account for an important proportion of oceanic primary production and usually dominate the arctic microplankton community during spring blooms (e.g., Tréguer *et al*. 2018; Lalande *et al.* 2019). Their silicified cell walls (i.e. frustules) exhibit a large morphological diversity (size, shape, level of silicification, etc.), which gives them differential sinking and sedimentary preservation potential. Their short generation time and largely species-specific response to environmental conditions make them useful indicators of changes in sea-surface conditions. While some diatoms thrive in the bottom layer of sea ice, a seasonal succession of taxa typically follows sea-ice breakup leaving a unique, though fragmentary, environmental signature in the underlying sediment. Following nutrient exhaustion, fast-growing genera, including *Chaetoceros*, can produce a rain of small, highly silicified and fast-sinking resting spores that preserve well in the sediment and attest to past productivity levels (Abelmann *et al*. 2006). Subfossil diatom abundance and assemblage composition can thus be used to infer information about past primary production and its link to climate-sensitive parameters, including sea-ice.

Samples for diatom analyses were prepared using ca. 0.3 g of dry sediment and following the standard methodology described in Crosta *et al.* (2020; S1). Quantification was done using a light microscope (Olympus BX53) with phase contrast optics, at 1000X magnification. Diatoms were analysed at a 4 to 28 cm sampling interval, which corresponds to an effective age resolution ranging from ca. 44 to 275 yrs (mean: ~115 yrs). *Chaetoceros* spores are not included in the relative abundance calculations.

Diatom concentrations were converted into fluxes by combining concentrations (valves or spores g^{-1}) with sediment densities derived from computed tomography (CT) numbers (or Hounslow units; Fortin *et al.* 2013) and accumulation rates derived from the age/depth model (cm yr^{-1}). Since the sediment

density was derived from CT numbers, fluxes are expressed as valves per unit of surface area per year, and while the trends can be compared, the flux values should not be directly compared with fluxes expressed in other units.

Fragilariopsis cylindrus and *Fragilariopsis nana* were grouped together (Plate 1). The fast-growing "marginal ice zone assemblage" is primarily represented by the cryopelagic *Fragilariopsis cylindrus, Fragilariopsis reginae-jahniae*, *Fragilariopsis oceanica* and *Fossula arctica*. All these taxa can be found in sea ice, but generally reach their highest abundances after ice breakup (von Quillfeldt 2004, Weckström *et al*. 2020). The "summer subsurface assemblage" comprises the large and highly silicified *Thalassiothrix longissima*, *Rhizosolenia* spp. (mainly *R. hebetata* f. *semispina* and *R. hebetata* var. *hebetata*) and *Coscinodiscus* spp. (notably *C. radiatu*s and *C. centralis*), whereas the "pack-ice/drift-ice assemblage" includes *Actinocyclus curvatulus* and *Melosira arctica* (Oksman *et al.* 2019).

3.2.3 Sea-ice biomarkers

The lipid biomarkers IP_{25} and HBI III are complementary indicators of past seasonal sea ice (e.g., Belt *et al.* 2007, 2013; Collins *et al.* 2013). IP_{25} is produced by at least three pan-Arctic diatom species (*Haslea spicula*, *Haslea kjellmanii*, and *Pleurosigma stuxbergii* var. *rhomboides*; Brown *et al.* 2014, Limoges et al. 2018a) that thrive in the bottom horizon of sea ice. This source-specific molecular compound is produced within the sea-ice matrix during the spring bloom and deposited in seafloor sediments following ice melt. In marine settings, high sedimentary IP_{25} contents are typically interpreted as indicating enhanced sea-ice concentrations, whereas the absence of IP_{25} in sediments can either reflect perennial sea-ice cover, ice-free conditions or insufficient production of source diatoms (e.g., Belt 2018, 2019). HBI III is known to be biosynthesised by diatoms belonging to the genera *Rhizosolenia*, *Pleurosigma* and *Haslea* (e.g., Belt *et al.* 2000, 2017; Rowland *et al.* 2001; Limoges *et al.* 2018a). Based on its distribution in surface sediments, HBI III has been proposed as an indicator of the receding sea-ice edge (Collins *et al.* 2013; Belt *et al.* 2015; Smik *et al*. 2016; Ribeiro *et al*. 2017), likely reflecting the neighboring open, fresh and stratified water of the marginal ice zone.

Koch *et al.* (2020), however, also reported production of HBI III in the Bering and Chukchi Sea starting during the spring under-ice diatom bloom, although peak production was recorded in September.

Sediment samples for sea-ice biomarker (IP_{25} and HBI III) analysis were processed according to the protocol described by Belt *et al.* (2007; S1). The data were collected using ChemStation and analyzed using MassHunter quantification software. HBIs were identified on the basis of retention time and comparison of mass spectra with authenticated standards. IP_{25} and HBI III abundances were obtained by comparison of individual GC-MS responses against those of the internal standard and concentrations are reported in ng g^{-1}. Response factors of the internal standard vs. IP_{25} were determined prior and after each analytical sequence (every 15 samples). The seasonal sea-ice biomarkers were analysed at a 1 to 10 cm sampling interval, which corresponds to an effective age resolution ranging from ca. 12 to 165 yrs (mean: ~33 yrs).

4. Results

4.1 TOC, TN, $\delta^{15}N$ and $\delta^{13}C$

TOC contents remain low and range between 0.59 and 1.52 wt% (S2). The lowest values were measured in the lowermost portion of the core. They then increase sharply to ca. 1 wt% around 7.7 kyrs BP (Figure 3). Following this rapid increase, values continue to slowly rise before stabilizing starting around 5 kyrs BP to values oscillating around 1.4 wt%. This translates into low TOC fluxes from 9.2 to 7.7 kyrs BP. TOC fluxes then show a stepwise increase to reach maximum values between 6.6 and 6 kyrs BP. From 6 kyrs BP fluxes decrease stepwise until 3.2 kyrs BP, from which point they drop to low values that are comparable to those observed between 9.2 and 7.7 kyrs BP. From ca. 1.4 kyrs BP, TOC fluxes slowly increase towards the top of the core. Total nitrogen (TN) contents varies between 0.08 and 0.18 wt%. The lowest values are also found from the bottom of the core until 7.7 kyrs BP, from which point they are generally increasing. These translate into TOC:TN ratios ranging from ca. 5 to 9 (Figure 4).

Nitrogen isotopic compositions range from 6.88 to 8.21 ‰ (Figure 3, S2), similar to the nitrogen isotopic signature of modern surface and sub-surface nitrates in central and western Baffin Bay (Lehmann *et al*. 2019). $\delta^{15}N$ values increase rapidly from 6.88‰ from the bottom of the core to reach a peak (8.21‰) at 8.5 kyrs BP, and then decrease until 8 kyrs BP. $\delta^{15}N$ values subsequently rise until 7 kyrs BP, from which point they decrease progressively until 5 kyrs BP (Figure 3). The nitrogen composition of organic matter thereafter remains relatively constant towards the top of the core, with an average value of 7.11‰. Carbon isotopic values range from –21.89 to –24.40‰ (Figure 3, S2). Values are increasing from the bottom of the core, until ca. 3 kyrs BP when they reach a plateau and remain high (~ –22%). From 1 kyrs BP, values show a general decreasing trend (Figure 3).

4.2 Diatoms

A total of 60 diatom taxa were identified (S3). Diatom concentrations range from <1 to ca. $6x10^7$ valves g^{-1} dry sediment, which translates into fluxes between ca. 0 to $4x10^9$ valves surface $area^{-1}$ yr^{-1} (S4). Our data reveal a strong temporal variability in Holocene diatom fluxes, with a 24x difference between the lowest and peak diatom fluxes.

Changes in the diatom fluxes are accompanied by clear compositional shifts in the assemblages (Figure 5). The bottom of the core (9.2 to 7.7 kyrs BP) is characterized by the lowest fluxes of diatom valves and moderate fluxes of *Chaetoceros* spores (Figures 5-6). The assemblage has a unique composition, with high contribution of the marginal ice zone group and the maximum relative abundance of *Fragilariopsis oceanica* (20%), *Thalassiosira nordenskioeldii* (7%), and presence of *Thalassiosira bulbosa* (<2%). Around 7.2 kyrs BP, an ephemeral peak in the abundance of *Actinocyclus curvalus* is observed, while the contribution of the marginal ice zone group decreases. Total diatom fluxes remain relatively low until 6 kyrs BP and then progressively increase to reach maximal values at around 4.4 kyrs BP. Increasing diatom fluxes are associated with an increase in the abundance of *T. antarctica* var. *borealis* (resting spore), which largely dominates the assemblages. After 4.4 kyrs BP, a stepwise decrease in total diatom fluxes is observed. At the same time, the

assemblages show a decrease in the relative abundances of *T. antarctica* var. *borealis* (resting spore) and a strong increase in the marginal ice zone taxa. At 3 kyrs BP, an abrupt and pronounced decline in the total diatom fluxes is accompanied by a rapid shift to a new regime of diatom productivity: a sharp decline in the marginal ice zone assemblage concurs with a marked increase in the share of the "drift-ice/pack-ice" and "summer subsurface" taxa. Although still a dominant contributor to the assemblages, *T. antarctica* var. *borealis* (resting spores) shows lower relative abundances from 3 kyrs BP. Relatively low diatom fluxes, with slight oscillations, prevail for the rest of the core record. However, fluxes were particularly low between 3 to 2 kyrs BP. From 2 kyrs BP, a progressive increase in *Rhizosolenia* spp. is observed, whereas the contribution of *T. longissima,* occupying the same ecological niche, decreases to moderate values. The share of both the "drift-ice/pack-ice" and "summer subsurface" assemblages remains high for the rest of the core.

4.3 Sea-ice biomarkers

The sea-ice biomarker IP_{25} was detected throughout the entire record, attesting to the presence of a seasonal sea-ice cover in the study area over the past 9.2 kyrs BP. Fluxes of IP_{25} are moderately high at the bottom of the core, increase starting from 7.8 kyrs BP, peak at around 7.4 kyrs BP and then progressively decrease from 6.6 until to 4.4 kyrs BP (Figure 3, S5). A slight increase in the IP_{25} fluxes is also observed between 3.9 and 3.2 kyrs BP. Between 3.2 and 1.5 kyrs BP, IP_{25} reaches its lowest values. Following this interval, IP_{25} rises again to reach a maximum around 0.2 kyrs BP.

The earliest peak in IP_{25} is followed by an increase in HBI III fluxes starting around 7 kyrs BP. HBI III remains relatively high until 6.1 kyrs BP and declines for about 600 years before increasing slightly again at 5.5. kyrs BP (Figure 3, S5). Generally low HBI III fluxes after 5.1 kyrs BP are concurrent with the decline in IP_{25}. During the interval between 5.1 and 2.3 kyrs BP, variations in HBI III and IP_{25} are synchronous. However, a sharp increase in HBI III at 2.3 kyrs BP marks an interval of sustained higher HBI III values. HBI III increases sharply from ca. 0.25 kyrs BP towards the surface. Notably, the major increase in HBI III from 2.3 kyrs BP is concurrent with a marked

increase in the relative abundance of the HBI III-producing species *Rhizosolenia hebetata* f. *semispina* (Belt *et al.* 2017; Figure 3).

5. Discussion

5.1 Primary production and sea-ice dynamics on the Northwest Greenland shelf

As illustrated by previous studies based on dinoflagellate cysts, foraminiferal assemblages and geochemical data (Caron *et al.* 2019; Hansen *et al.* 2020; Giraudeau *et al.* 2020), core AMD14-204 captures the Holocene post-glacial climate development off northwest Greenland. The continuous and high-resolution multiproxy record presented here allows us to infer detailed information about changes in seasonal sea ice and primary production.

Low productive environment, extensive sea-ice cover, land-sourced meltwater influence and deglacial opening of Nares Strait **(ca. 9.2 - 7.7 cal kyrs BP)**

The low organic carbon, low HBI III and moderate IP_{25} fluxes in the lowermost part of the core suggest a prolonged sea-ice season and low productivity. Fluxes of *Chaetoceros* spores are moderate but otherwise diatom valve fluxes are much reduced (about three times below the core average). This interval notably shows a high contribution of the marginal ice zone group (Figure 6) and the highest relative abundance of *Thalassiosira nordenskioeldii*. This species typically reaches its highest relative abundance after ice break-up and is thought to be a late-spring bloomer (Oksman *et al.* 2019). Intermediate abundances of *T. antarctica* var. *borealis* (resting spore) additionally suggest cold, open-water conditions during summer. The production of *Chaetoceros* spores generally represents the last stage of the diatom growth season and is initiated by nutrient exhaustion in the surface water (McQuoid and Hobson, 1996). Some *Chaetoceros* species that are lightly silicified can more easily take up nutrients and can maintain populations in nutrient-depleted waters (Booth *et al.* 2002). The high $\delta^{15}N$ values, along with low TOC and diatom fluxes, are coherent with a scenario of limited surface water nitrate availability and late sea-ice breakup. At the closely located core GeoB19927, the IP_{25} and HBI III trends are comparable to ours, and brassicasterol and dinosterol fluxes show relatively high but decreasing values from ca. 9.5 to 7.8 kyrs BP (Saini *et al.* 2020). While our proxy

signals may have been somewhat diluted by elevated clastic input during this interval, all proxies nonetheless point towards a low to moderately productive environment. This agrees with the extensive sea-ice cover, marked meltwater and detrital sediment discharges also documented by Caron *et al* (2019), and low entrainment of Atlantic water into the WGC inferred from foraminiferal assemblages (Hansen *et al.* 2020), during an interval of rapid thinning of the Melville sector of the Greenland Ice Sheet (Giraudeau *et al.* 2020). It is also between ca. 9-8.3 kyrs BP that the retreat of the Greenland and Innuitian ice sheets led to the complete opening of Nares Strait (Georgiadis *et al.* 2018, Jennings *et al.* 2019), establishing a new oceanic connection between the Arctic Ocean and Baffin Bay and a new source of Pacific-derived waters into northern Baffin Bay. The increase in the $\delta^{15}N$ values recorded from ca. 8.4 kyrs BP is coherent with the advection of isotopically heavier Pacific water into Northern Baffin Bay.

Increasing primary production, stratified water column and onset of WGC influence **(ca. 7.7 – 6 cal kyrs BP)**

From 7.7 kyr BP, a steep increase in the sedimentary TOC contents indicates either a transition to a more productive system and/or reduced detrital input from meltwater. This TOC flux increase is coeval with a WGC strengthening inferred from the mineralogical and elemental composition of the sedimentary material (Caron *et al.* 2020), and enhanced abundance of foraminiferal species indicative of Atlantic Water influx at our study site (Hansen *et al.* 2020) (Figure 6). From ca. 7 kyrs BP, a progressive strengthening of the WGC has also been recorded in Disko Bay (e.g., Perner *et al.* 2012; Ouellet-Bernier *et al.* 2014) and attributed to the onset of deep-water formation in the Labrador Sea (Hillaire-Marcel *et al.* 2001), presumably linked to a basin-wide reorganization of the surface circulation in the northern Atlantic following the final retreat of the Laurentide and Greenland ice sheets (Dyke and Prest 1987; Van Nieuwenhove *et al.* 2016, 2018). An increase in IP_{25} fluxes accompanied by a peak contribution of *A. curvatulus*, a species strongly associated with heavy pack-ice in northern Baffin Bay (Williams 1986, 1990), likely further suggest an episode of heavier sea-ice cover centered at ca. 7.2 kyrs BP.

Between 7 and 6 kyrs BP, a clear excursion in the HBI III fluxes is coeval with a punctual increase in diatom fluxes, a sharp decline in the Atlantic Water foraminiferal species (Hansen *et al.*

2020) (Figure 6) and a short-lived peak in the ice-rafted debris (IRD) content (Caron *et al.* 2018) at our study site. During this interval, the marked contribution of ribbon-forming pennate *Fragilariopsis cylindrus* and *F. reginae-jahniae* — two spring bloomers associated with ice melt (e.g., von Quillfeldt 2001)— attests to cold, low-salinity spring/early summer conditions. High dinosterol fluxes at site GeoB19927 suggest sustained high dinoflagellate productivity from ca. 7.4 kyrs BP (Saini *et al.* 2020). From 7 kyrs BP Caron *et al.* (2019) documented a slight decrease in the dinoflagellate cyst fluxes accompanied by a decline in the phototrophic taxon *Operculodinium centrocarpum*. Diatoms and dinoflagellates have distinct life-cycle strategies, involving different environmental and ecophysiological optima (e.g., Litchman and Klausmeier, 2008). Here, the phytoplankton signal (diatoms and dinoflagellates) may point towards a productive vernal bloom, followed by a relatively short phytoplankton growth season and/or stratified water column. In the Kane Basin, increased HBI III fluxes were recorded during this interval (core AMD14-Kane2B, Georgiadis *et al.* 2020), suggesting increased mobile sea-ice and freshwater outflow via Nares Strait. Coherent with the high $\delta^{15}N$ and HBI III values, enhanced outflows of Arctic waters may have contributed to the already well-stratified waters resulting from continued meltwater input from the Greenland ice sheet. As suggested by Hansen *et al.* (2020) the input of highly saline corrosive deep Arctic water or brines may have impeded the growth (or preservation) of benthic calcareous foraminifera at our study site during this interval.

From primary production optimum with increased Atlantic signature of the WGC, to Neoglacial cooling and re-establishment of persistent seasonal sea ice **(ca. 6-3 cal kyrs BP)**

In phase with a progressive decline in IP_{25}, suggesting a transition to earlier seasonal sea-ice retreat, diatom production rises markedly until ca. 4.4 kyrs BP. At core GeoB19927, this is associated with sustained high dinosterol fluxes (Saini *et al.* 2020). During this interval, diatom assemblages are largely dominated by the centric species *T. antarctica* var. *borealis* (resting spore), with low contributions of the marginal ice zone group (Figure 6). In modern water samples from West Greenland, the occurrence of *T. antarctica* var. *borealis* resting spores was linked to higher surface water temperatures, and on the Holocene timescale, based on sediment assemblages, it was linked to the influence of temperate WGC waters (e.g., Krawczyk *et al.* 2010, 2013, 2014, as *T. kushirensis*).

Additionally, while diatom production progressively increases, $\delta^{15}N$ values decline from the beginning of this interval until they reach a plateau at 4.8 cal kyrs BP. This signal can suggest increasing nitrate supplies to the surface water due to reduced stratification. A reduced stratification would be consistent with reduced meltwater input from the Greenland Ice Sheet following the early Holocene (Giraudeau *et al.* 2020). Along northwest Greenland, the ice margin reached its minimum extent between ~5 and 3 kyrs BP (Briner *et al.* 2014) and reduced meltwater runoff was inferred after 6 kyrs BP (Moros *et al.* 2016 and references therein). Overall, this interval shows a progression to a longer duration of the open-water growth season and surface conditions favorable to primary production, which could further be linked to the inferred generally warmer and strengthened WGC during this interval (Jennings *et al.* 2002, 2011, 2014; Perner *et al.* 2013; Hansen *et al.* 2020). It is worth noting that low amplitude peaks in HBI III were always coeval with events of reduced Atlantic benthic foraminifera species at the study site (Hansen *et al.* 2020), possibly indicating episodes of decreased advection of Atlantic Water, and increased water column stratification or polar inflows.

After 4.4 kyrs BP, the long-term decline in IP_{25} ceases and diatom production declines stepwise. The same declining trend is observed in the dinosterol content of core GeoB19927 (Saini *et al.* 2020). A gradual increase in the contribution of the marginal ice zone diatom group (Figure 6) hints at a progressive return to colder conditions, while higher $\delta^{13}C$ values suggest increased contribution of ice-derived organic matter to the sediments (Figure 4). These changes coincide with the inception of a stable and recurrent North Water polynya dated to ca. 4.4 cal kyrs BP (Davidson *et al*. 2018). This timing also coincides with a snowline lowering across 15 different ice caps in central West Greenland, which has been interpreted to reflect persistent summer cooling (Schweinsberg *et al.* 2017). During the entire interval, short-term increases in HBI III fluxes were synchronous with low amplitude rises in IP_{25} fluxes, suggesting that the orbitally-driven long-term Neoglacial cooling (Vinther *et al.* 2009) associated with decreasing summer insolation in the Northern Hemisphere was interrupted by short events of fluctuating sea-ice conditions at the study site. Starting around 3.5 kyrs BP, the major increase in the contribution of the marginal ice zone group, and especially *F. reginae-jahniae,* suggests the re-establishment of more persistent seasonal sea ice (Weckström *et al.* 2020; Figure 6). Interestingly, this is synchronous with an increase in the dinoflagellate productivity reported at core GeoB19927 (Saini *et al.* 2020), and marked increase in the dinoflagellate cyst fluxes,

notably involving a decline in *Operculodinium centrocarpum* and steady increase in the spring bloomer *Pentapharsodinium dalei* at our study site (Caron *et al.* 2019). Such high contribution of the marginal ice zone diatom assemblage, high abundance of the Atlantic benthic foraminiferal species and high fluxes of dinosterols and dinoflagellate cysts in the study area may indicate a change in sea-ice seasonality and an increased proximity of the study site to the spring marginal ice edge.

***Primary production decline, extensive sea-ice cover, stratified water column and weakened Atlantic water signature of the WGC* (ca. 3.0 - 1.2 cal kyrs BP)**

We record an abrupt change in the diatom regime taking place at 3 kyrs BP. IP_{25}, HBI III and diatom fluxes (including *Chaetoceros* spores) decline to minimum values at the beginning of this interval. A steep decline in the contribution of the marginal ice zone group is shortly followed by a pronounced increase in the "drift-ice/pack-ice" and "summer subsurface" assemblages (Figure 6). The drift-ice/pack-ice assemblage includes *Melosira arctica*, a species known to form dense aggregates under sea ice, which can be abundant under drift ice and has been observed to form free-floating filaments in the meltwater layer of the Arctic Ocean (von Quillfeldt *et al.* 2003, Poulin *et al.* 2014). It secretes gelatinous extracellular polysaccharide substances that facilitate its anchoring to the ice matrix (Krembs *et al.* 2011) and has been linked with widespread spore formation following nutrient depletion and grazing activities towards the end of the spring bloom in Baffin Bay (Lafond *et al.* 2019). In surface sediments and sediment traps from Greenland, *M. arctica* is strongly associated with spring/summer sea ice (Krawczyk *et al.* 2017, Luostarinen *et al.* 2020). The drift-ice/pack-ice assemblage also includes *Actinocyclus curvatulus,* a cold-water species that is associated with high sea-ice concentrations (Oksman *et al.* 2019) and heavy pack ice in northern Baffin Bay (Williams 1986, 1990). The summer subsurface assemblage includes the genus *Coscinodiscus,* containing species known to thrive at low light irradiance levels under pack ice (Kemp *et al.* 2000, Duerksen *et al.* 2014), and contributing substantially to the early spring bloom in the North Water polynya (Lovejoy *et al.* 2002). Outside of the polar regions, *Coscinodiscus* spp. (such as the dominant *Coscinodiscus* species in our study) are an important constituent of the subsurface chlorophyll maximum (Odebrecht and Djurfeldt, 1996; Weston et al, 2005). This assemblage also comprises *Rhizosolenia* sp. and *Thalassiothrix longissima*. Both Rhizosolenids and *Thalassiothrix* spp. have

been documented to thrive in zones of converging surface currents: their capacity to regulate buoyancy, exploit deep nutrient sources and reproduce at low light conditions, make them adapted to a stratified water column (e.g., Kemp *et al.* 2006 and references therein). *Thalassiothrix longissima,* which yielded its maximum abundance (~4%) during this interval*,* is further associated with relatively warm summer open-water conditions (Knudsen *et al.* 2008, Oksman *et al.* 2019), and marine to brackish conditions (Pearce *et al.* 2014). Albeit distinct from the rest of the core, this diatom assemblage has a strong sea-ice fingerprint.

Between 3.2 and 2.3 kyrs BP, the sharp decline in primary production inferred here concurs with significant worldwide glacier advances (e.g., Grove 2004, Wanner *et al.* 2008). Regionally, it is concomitant with inferred climate deterioration in northern Baffin Bay (Levac *et al.* 2001, Knudsen *et al.* 2008, St-Onge and St-Onge 2014), marked reduction in the meltwater discharge at 3.2 kyrs BP in southwestern Greenland fjords (Møller *et al.* 2006, Seidenkrantz *et al.* 2007), a major temperature drop in Jakobshavn Isbræ at ca. 3 kyrs (Young and Briner 2015) and shift towards cooler conditions in Disko Bay from 3.5 to 2.6 kyrs BP (Moros *et al.* 2016). Additionally, Thomas *et al.* (2016) reported a steady decrease in winter snowfall in western Greenland from 4.4 to 2 kyrs BP, implying a more extensive sea-ice cover that limited not only moisture availability but also primary production during this interval. In this context, our low IP_{25} flux values appear puzzling. A similar low IP_{25} signal from the neighboring core GeoB19927 has been interpreted to reflect low sea-ice concentrations under the influence of a persistent WGC (Saini *et al.* 2020). However, this interpretation is difficult to reconcile with the overall low primary production, relatively high organic matter $\delta^{13}C$, sudden decrease in the contribution of planktonic and benthic Atlantic Water foraminiferal species at the study site (Hansen *et al.* 2020) and low dinocyst fluxes dominated by cysts of the spring bloomer *Pentapharsodinium dalei* (Caron et al. 2019). Our proxy record suggests that conditions other than sea-ice presence may have affected the growth of IP_{25}-producing species or IP_{25} biosynthesis during this interval. Changes in nutrient availability can exert a major control on total primary production and influence the cellular HBI-synthesis in diatoms (Brown *et al.* 2020). Considering that the assemblages are composed of large diatoms that typically benefit from higher nutrient levels (i.e. larger diffusion boundary layer), the hypothesis of a decrease in the nutrient availability is unlikely. Alternatively, a change in the ice matrix linked to reduced sea-surface salinity may have impacted the settlement efficiency and growth

of IP_{25}-producing sympagic algae (Poulin e*t al.* 1983, Gosselin *et al.* 1986) as seen in coastal sediments and sea ice from Greenland fjords (Ribeiro *et al.* 2017, Limoges *et al.* 2018a, 2018b). This could partly explain the presence of sub-ice colonial species such as *M. arctica* that have developed strategies to mitigate the effect of unfavorable sea-ice microstructure (Krembs *et al.* 2011). To the north, evidence of instabilities in the Kane Basin ice arch (Georgiadis *et al.* 2020) may suggest progressively increasing outflow of freshwater into northern Baffin Bay from 3 kyrs BP. As also raised by Hansen *et al.* (2020), an increased polar influence was documented in other cores from the Labrador shelf (Gibb *et al.* 2015; Lochte *et al.* 2019). The observed shift to giant and highly silicified diatom taxa observed here would further support increased input of Pacific waters high in nutrients (especially Si and P) and/or decreased upstream nutrient uptake. Our data caution for the use of sedimentary IP_{25} as a sole indicator for past fluctuations in sea-ice and suggest that ice-laden conditions persisted into the growing season of diatoms despite low sedimentary IP_{25} values. Furthermore, we argue that the drastic changes in the diatom species composition and production reflect an important oceanographic reorganization during this interval (see section 5.2).

From 2.3 to 1.2 kyrs BP, HBI III increases sharply and the diatom assemblages show a progressive increase in *Rhizosolenia* spp. and *F. cylindrus*, and a decrease in *T. longissima*. The proxy-signal suggests enhanced surface-water cooling and freshening during this interval, likely partly associated with increased meltwater input. This is supported by the observed increase in IRD between 2.3 and 2 kyrs BP at our study site (Caron *et al*. 2020), and is coherent with the retreat of the Qangattaq ice cap on the Nuussuaq peninsula between ca. 2.5 and 1.9 kyrs BP (Schweinsberg *et al*. 2017) and the Greenland ice-sheet margin in Northern Nunatarssuaq between 2.1 and 1.6 kyrs BP (Farnsworth *et al.* 2018), at the transition to a period of significant boreal atmospheric warming that is commonly referred to as the Roman Warm Period (~2.0-1.65 kyrs BP, Wanner *et al.* 2008). Biomarker and foraminiferal datasets further suggest the potential complete collapse of the Kane Basin ice arch in Nares Strait during this interval (Georgiadis *et al.* 2020), which would have further promoted the export of freshwater and (multiyear) ice into northern Baffin Bay.

Low primary production, extensive but fluctuating sea-ice conditions **(ca. 1.2 −0.2 cal kyrs BP)**

The last 1.2 kyrs BP were characterized by a marked increase in IP_{25} and generally stable HBI III fluxes, high contribution of the pack-ice/drift-ice and summer subsurface assemblages, moderate contribution of the marginal ice zone assemblage, and relatively high organic matter $\delta^{13}C$ values, suggesting the presence of an overall extensive, but fluctuating sea-ice cover (Figures 4-6). While diatom fluxes remain low for the complete interval, the signal is overprinted by high frequency events of low amplitude increase and decrease in diatom production. Saini *et al.* (2020) also reported low brassicasterol and dinosterol fluxes. Collectively, the diatom, brassicasterol and dinosterol signals contrast with the high primary productivity reconstructed using the dinoflagellate cyst-based modern analogue technique (MAT) (Caron *et al.* 2019). We hypothesize that the MAT signal is steered by the dominance (50-60%) of cysts of the phototrophic species *Pentapharsodinium dalei*, which often occurs in large numbers in the productive waters of the early-season bloom, but whose intense, transient pulses of cyst production rather seem to be favoured by the highly stratified waters resulting from ice melt (e.g., Howe *et al.* 2010, Heikkilä *et al.* 2014). During this interval, low primary production would have resulted from a relatively extensive seasonal sea-ice cover and comparatively short open-water season during an interval of generally cold atmospheric temperatures (Lasher *et al.* 2017, Lecavalier et al. 2017). A re-advance of the Upernavik Isstrøm was dated to ca. 0.6 kyr BP (Briner *et al.* 2013). At the top of the core, the sharp increase in HBI III and *Rhizosolenia* spp. hint at a possible return to more stratified conditions and increased freshwater influence.

5.2 Impact of millennial-scale AO variability on primary production

Millennial and centennial variations in the dominant atmospheric mode have been identified in various studies. These are based on, to name a few, indicators of sea-ice drift patterns in the Arctic Ocean, such as ice-rafted iron in the Beaufort Sea (Darby *et al.* 2012) and the abundance and origin of driftwood on the Northern Greenland shores (Funder *et al.* 2011), as well as tracers of exceptional rainfall events in North American lakes (Noren *et al.* 2002). While a dominantly positive AO phase was suggested for the northern Greenland Holocene Thermal Maximum between 8.5-6 kyrs BP (Funder *et al.* 2011), it is only by ~6.8 kyrs BP that modern-type ocean surface circulation presumably was established in the North Atlantic (Van Nieuwenhove *et al.* 2018). Given this and the

lower resolving power of the diatom analyses (due to low diatom valve concentrations) in the lower part of our core (9.2 to 6 kyrs BP), we refrain from linking our proxy record to a predominant atmospheric circulation pattern during this interval. We however reconstruct moderate diatom production associated with increased Arctic water and drift-ice influence, and a stratified water column. From 6 kyrs BP and as solar irradiance decreases, we note that the onset of a 3000-year phase of dominantly negative AO (Darby *et al.* 2012; Funder *et al.* 2011; Staines-Urías *et al.* 2013) is associated with sustained higher diatom fluxes and abundance of Atlantic benthic foraminiferal taxa. The proxy signal suggests a longer duration of the open-water growth season and generally warmer and strengthened WGC during this interval. The initial phase of the Neoglacial cooling was then marked by the establishment of progressively more extensive spring sea ice, which translated into a stepwise overall decrease in primary production starting at 4.4 kyrs BP and sharp increase in the dominance of spring marginal ice zone taxa.

The diatom productivity collapse documented at 3 kyrs BP is coeval with fluctuations reported from several other areas of the northern North Atlantic region (e.g., Rasmussen *et al.* 2002; Jennings *et al.* 2011; Douarin *et al.* 2016), implying a large-scale oceanographic reorganization. This important cooling event was further associated with a slowdown of the Atlantic Meridional Overturning Circulation around 3.1–2.4 kyrs BP (Oppo *et al.* 2003). As summarized by Morley *et al.* (2014), this shift is thought to be partly associated with a strengthened EGC provoking a southeastward movement of the subarctic front and longitudinal stretching of the subpolar gyre. This cooling event coincides with a swing from persistently negative to positive AO at ca. 3 kyrs BP (Funder *et al.* 2011, Darby *et al.* 2014) (Figure 6), reinforcing the hypothesis that millennial-scale AO-driven changes in ocean conditions may have prompted changes in sea ice and primary production off northwest Greenland during the mid-to-late Holocene. While positive winter AO is typically associated with colder than normal atmospheric temperatures in West Greenland (Box 2002), the long-term decreased contribution of the warm Irminger Current into the WGC (e.g., Flatau *et al*. 2003; Sarafanov 2009; Andrews and Jennings 2014; Morley *et al*. 2014) may have exacerbated atmospheric cooling along the West Greenland margin from 3 kyrs BP (Figure 7). Such a reduction of Atlantic-sourced water to the WGC from 3 to 2.3 kyrs BP would have contributed to later sea-ice melt. This hypothesis is supported by the major decline in both the Atlantic water foraminiferal species (Hansen *et al.* 2020)

and the relatively warm sea-surface indicator dinoflagellate cyst *Operculodinium centrocarpum* (Caron *et al.* 2019) at our study site. To the north, evidence of instabilities in the Kane Basin ice bridge from 3 kyrs BP (Georgiadis *et al.* 2020) also suggests progressively increasing outflow of polar freshwater into northern Baffin Bay. Increased input of nutrient-rich (particularly Si) polar water would have promoted the large and highly silicified diatom flora while also contributing to a stratified upper water column. The resulting ice-laden and stratified waters, and short growth season would have led to the major decline in primary production.

At 2.3-2 kyrs BP, Darby *et al.* (2014) inferred an episode of unprecedented high positive AO for the Holocene (Figure 6), which coincides with a major increase of HBI III at our study site. During this episode, the lowest sea-ice concentrations were inferred at Kane Basin, suggesting that the Kane Basin ice bridge was much weakened (Georgiadis *et al.* 2020), presumably impacting the functioning of the North Water polynya. While no modern analog exists for an AO event of this amplitude, we hypothesize that it may have resulted in important exports of drift ice and polar waters via Nares Strait. It is further notable that this event shortly preceded the onset of the Roman Warm Period, which was coeval with a return to weaker AO (Darby *et al.* 2014), decreased polar water influence in the subpolar North Atlantic (Moffa-Sánchez and Hall 2017) and slightly increased productivity at the study site. Our proxy record suggests that this connectivity between persistent AO phase and large-scale oceanography has also prevailed during the late Holocene and, superimposed on radiative changes, likely played a key role in the Baffin Bay oceanography, and in the onset and length of the open-water growth season along the West Greenland margin, with consequences for microalgal production and phenology.

5.3 Future evolution of marine primary production

Our proxy record suggests that over the last 9000 years, modulations in millennial-scale AO modes have been linked to the variability in sea ice and diatom production on the Northwest Greenland shelf by exerting a control on the physico-chemical conditions of the water column (e.g., thermal stratification, glacial meltwater input, nutrient supply, sea-ice regime). Since it is generally assumed that climate warming in the Arctic will cause an earlier vernal bloom and extend the open-water

growth season, it can be tempting to predict a future increase in primary production, similar to that observed between 6 and 4.4 cal kyrs BP in our study area. During this interval, phytoplankton production (diatoms and dinoflagellates) appears to have been promoted by the enhanced entrainment of Atlantic water by the WGC and earlier sea-ice break-up during a predominantly negative AO phase. However, since studies suggest that the Arctic warming and the Arctic Amplification (e.g., Manabe and Wetherald 1975, Serreze *et al.* 2009) may favor positive-like AO conditions, notably associated with a wavier flow of tropospheric circulation and more frequent extreme winter weather conditions in the North Hemisphere mid-latitudes (Cohen *et al.* 2018), neither the highly productive interval from 6-4.4 cal kyrs BP, nor any other Holocene interval can be regarded as a direct analog for the future. Instead, earlier and rapid seasonal sea-ice melt may affect the timing and production of fast-growing sea ice-associated taxa (e.g., Tedesco *et al.* 2019). Additionally, our long-term record clearly shows that thermal and freshwater-induced upper water column stratification resulting from atmospheric warming, increased glacial meltwater input and polar water/drift-ice throughflows such as those taking place during positive AO intervals and predicted to increase in a warming Arctic, have a strong impact on community structure and are generally detrimental to diatom productivity. Hence, future diatom productivity in the area will be modulated by the balance between the effects of a longer open-water growth season *versus* the effects of an enhanced water column stratification. This will certainly result in changes in microalgal community structure and phenology.

6. Conclusions

Our multiproxy record supports the hypothesis of a pervasive effect of the dominant AO phase on sea-ice conditions and diatom production on the northwest Greenland shelf. Most notably, we show that an important and rapid decline in primary production starting around 3 cal kyrs BP was coeval with a shift from low to high AO polarity values.

Changes in sea ice and diatom productivity over the past 9000 years on the Northwest Greenland shelf can be summarized as follows:

1) Extensive seasonal sea-ice cover from 9.2 to 7.7 cal kyrs BP associated with low to moderate diatom production during an interval of significant meltwater influence and deglacial opening of the Nares Strait gateway.
2) Polar Water outflow event centered at ca. 6.6 cal kyrs BP associated with increased HBI III fluxes and a moderately high diatom production.
3) Progressive decline in seasonal sea-ice concentrations from 6 cal kyrs BP culminating with primary production optimum.
4) Onset of the Neoglacial cooling at ca. 4.4 cal kyrs BP accompanied with progressively increasing sea-ice concentrations and decreasing phytoplankton production.
5) Major shift in diatom productivity at 3 cal kyrs BP reflecting a major oceanographic reorganization presumably related to a swing from dominantly negative to positive AO. Resulting decrease in the Atlantic-sourced influence of the WGC and increase in Arctic throughflows likely led to a shorter open-water growth season and generally reduced primary production. These conditions were exacerbated from 2.3 to 2 cal kyrs BP during an interval of record-high positive AO.
6) From 1.2 to 0.2 cal kyrs BP, only slight oscillations in diatom production and generally extensive seasonal sea-ice cover occurred during an interval of dominantly negative AO.

7. Data Sharing and Accessibility Statement

The data that supports the findings of this study are available in the supplementary material of this article. Subfossil diatom counts are also openly available in PANGAEA at (doi), PDI-25282.

8. Acknowledgements

Core AMD14-204 was collected as part of the GreenEdge project funded by ANR and the Total Foundation. Ship-time was funded by the ERC-STG-ICEPROXY project. We acknowledge the help of Drs. Guilmette and Van Nieuwenhove for biomarker analyses and in picking foraminifera. We thank Drs. Darby and Caron for providing IRD and dinocyst data. This project was funded by FRQNT (188947) and NSERC-DG (2018-03984) grants to AL. MSS was funded by the Danish Council for Independent Research (7014-00113B/FNU; G-Ice project).

REFERENCES

Abelmann A, Gersonde R, Cortese G, Kuhn G, Smetacek V (2006). Extensive phytoplankton blooms in the Atlantic sector of the glacial Southern Ocean. Paleoceanography 21, PA1013.

Andersen C, Koç N, Jennings A, Andrews JT (2004). Nonuniform response of the major surface currents in the Nordic Seas to insolation forcing: Implications for the Holocene climate variability. Paleoceanography 19, PA2003.

Andrews JT and Jennings AE (2014). Multidecadal to millennial marine climate oscillations across the Denmark Strait (~66°N) over the last 2000 cal yr BP. Clim. Past 10, 325-343.

Arrigo KR and van Dijken GL (2015). Continued increases in Arctic Ocean primary production. Progress in Oceanography, 60-70.

Arrigo KR, Perovich DK, Pickart RS, Brown ZW, van Dijken GL, Lowry KE, Mills MM, Palmer MA, Balch WM, Bahr F, Bates NR, Benitez-Nelson C, Bowler B, Brownlee E, Ehn JK, Frey KE, Garley R, Laney SR, Lubelczyk L, Mathis J, Matsuoka A, Mitchell G, Moore GWK, Ortega-Retuerta E, Pal S, Polashenski CM, Reynolds RA, Schieber B, Sosik HM, Stephens M, Swift JH (2012). Massive Phytoplankton Blooms Under Arctic Sea Ice. Science 336, 1408.

Belt ST, Allard WG, Massé G, Robert J-M, Rowland SJ (2000). Highly branched isoprenoids (HBIs): identification of the most common and abundant sedimentary isomers. Geochimica et Cosmochimica Acta 64, 3839-3851.

Belt ST, Massé G, Rowland SJ, Poulin M, Michel C, LeBlanc B (2007). A novel chemical fossil of paleo sea ice: IP_{25}. Organic Geochemistry 38, 16-27.

Belt ST, Brown TA, Ringrose AE, Cabedo-Sanz P, Mundy CJ, Gosselin M, Poulin M (2013). Quantitative measurement of the sea ice diatom biomarker IP_{25} and sterols in Arctic sea ice and underlying sediments: Further considerations for palaeo sea ice reconstruction. Organic Geochemistry 62, 33-45.

Belt ST, Cabezo-Sanz P, Smik L, Navarro-Rodriguez A, Berben SMP, Knies J, Husum K (2015). Identification of paleo Arctic winter sea is limits and the marginal ice zone: optimised biomarker-based reconstructions of late Quaternary Arctic sea ice. Earth and Planetary Science Letters 431, 127-139.

Belt ST, Brown TA, Smik L, Tatarek A, Wiktor J, Stowasser G, Assmy P, Allen CS, Husum K (2017). Identification of C25 highly branched isoprenoid (HBI) alkenes in diatoms of the genus *Rhizosolenia* in polar and sub-polar marine phytoplankton. Organic Geochemistry 110, 65-72.

Belt ST (2018). Source-specific biomarkers as proxies for Arctic and Antarctic sea ice. Organic Geochemistry 125, 277-298.

Belt ST (2019). What do IP_{25} and related biomarkers really reveal about sea ice change? Quaternary Science Reviews 204, 216-219.

Bergeron M and Tremblay JÉ (2014). Shifts in biological productivity inferred from nutrient drawdown in the southern Beaufort Sea (2003–2011) and northern Baffin Bay (1997–2011), Canadian Arctic. Geophysical Research Letter 41, 3979-3987. https://doi.org/10.1002/2014GL059649

Booth BC, Larouche P, Belanger S, Klein B, Amiel D, Mei Z-P (2002). Dynamics of *Chaetoceros socialis* blooms in the North Water. Deep-Sea Research II 49, 5003-5025.

Box JE (2002). Survey of Greenland instrumental temperature records: 1873-2001. International Journal of Climatology 22, 1829-1847.

Briner JP, Hakansson L, Bennike O (2013). The deglaciation and neoglaciation of Upernavik Isstrøm, Greenland. Quaternary Research 80, 459-467.

Briner JP, Kaufman DS, Bennike O, Kosnik M-A (2014). Amino acid ratios in reworked marine bivalve shells constrain Greenland Ice Sheet history during the Holocene. Geology 42, 75-78.

Brown TA, Belt ST, Tatarek A, and Mundy CJ (2014). Source identification of the Arctic sea ice proxy IP_{25}. Nature Communication. 5:4197. doi: 10.1038/ncomms5197.

Brown TA, Rad-Menéndez C, Ray JL, Skaar KS, Thomas N, Ruiz-Gonzalez C, Leu E (2020). Influence of nutrient availability on Arctic sea ice diatom HBI lipid synthesis. Organic Geochemistry 141, 103977.

Caron M, St-Onge G, Montero-Serrano J-C, Rochon A, Georgiadis E, Giraudeau J, Massé G (2018). Holocene chronostratigraphy of northeastern Baffin Bay based on radiocarbon and paleomagnetic data. Boreas, 147-165. DOI 10.1111/bor.12346

Caron M, Rochon A, Montero-Serrano J-C, St-Onge G. (2019). Evolution of sea-surface conditions on the northwestern Greenland margin during the Holocene. Journal of Quaternary Sciences 34 (7), 569-580.

Caron M, Montero-Serrano J-C, St-Onge G, Rochon A (2020). Quantifying provenance and transport pathways of Holocene sediments from the northwestern Greenland margin. Paleoceanography and Paleoclimatology. https://doi.org/10.1029/2019PA003809

Cohen J and Barlow M (2005). The NAO, the AO, and Global warming: how closely related? Journal of Climate 18, 4498-4513.

Cohen J, Pfeiffer K, Francis JA (2018). Warm Arctic episodes linked with increased frequency of extreme winter weather in the United States. Nature Communication 9, 869. https://doi.org/10.1038/s41467-018-02992-9

Collins LG, Allen CS, Pike J, Hodgson DA, Weckström K, Massé G (2013). Evaluating highly branched isoprenoid (HBI) biomarkers as a novel Antarctic sea-ice proxy in deep ocean glacial age sediments. Quaternary Science Reviews 79, 87-98.

Comeau AM, Li WKW, Tremblay J-E, Carmack EC, Lovejoy C (2011). Arctic Ocean microbial community structure before and after the 2007 record sea ice minimum. PLoS ONE 6(11), e27492. https://doi.org/10.1371/journal.pone.0027492

Crosta X, Shukla SK, Ther O, Ikehara M, Yamane M, Yokoyama Y (2020). Last Abundant Appearance Datum of Hemidiscus karstenii driven by climate change. Marine Micropaleontology 157, 101861.

Darby DA, Ortiz JD, Grosch CE, Lund SP (2012). 1,500-year cycle in the Arctic Oscillation identified in Holocene Arctic sea-ice drift. Nature Geoscience 5, 897-900. https://doi.org/10.1038/ngeo1629

[dataset]Limoges A, Weckström K, Ribeiro S, Georgiadis E, Hansen KE, Martinez P, Seidenkrantz M-S, Giraudeau J, Crosta X, Massé G (2020) Holocene biogenic sedimentary proxy record from the West Greenland shelf. PANGAEA. DOI to be assigned.

Davidson TA, Wetterich S, Johansen KL, Grønnow B, Windirsch T, Jeppesen E, Syväranta J, Olsen J, González-Bergonzoni I, Strunk A, Larsen NK, Meyer H, Søndergaard J, Dietz R, Eulears I, Mosbech

A (2018). The history of seabird colonies and the North Water ecosystem: Contributions from palaeoecological and archaeological evidence. Ambio 47, 175-192.

Douarin M, Elliot M, Noble SR, Moreton SG, Long D, Sinclair D Henry L-A, Roberts JM (2016). North Atlantic ecosystem sensitivity to Holocene shifts in Meridional Overturning Circulation. Geophys. Res. Lett. 43, 291-298.

Duerksen SW, Thiemann GW, Budge SM, Poulin M, Niemi A, Michel C (2014). Large, Omega-3 Rich, Pelagic Diatoms under Arctic Sea Ice: Sources and Implications for Food Webs. PLoS One 9(12), e114070.

Dyke AS, Prest VK (1987). Late Wisconsinan and Holocene history of the Laurentide ice sheet. Géographie physique et Quaternaire XLI, 237–263.

Farnsworth LB, Kelly MA, Bromley GRM, Axford Y, Osterberg EC, Howley JA, Jackson MS, Zimmerman SR (2018). Holocene history of the Greenland Ice-Sheet margin in Northern Nunatarssuaq, Northwest Greenland. Arktos 4: 10.

Flatau MK, Tally L, Niller PP (2003). The North Atlantic Oscillation, Surface Current Velocities, and SST Changes in the Subpolar North Atlantic. American Meteorological Society 16, 2355-2369.

Fortin D, Gebhardt AC, Hahn A, Kliem P, Lisé-Pronovost A, Roychowdhury R, Labrie J, St-Onge G (2013). Destructive and non-destructive density determination: method comparison and evaluation from the Laguna Potrok Aike sedimentary record. Quaternary Science Reviews 71, 147–153. doi:10.1016/J.QUASCIREV.2012.08.024

Funder S, Goose H, Jepsen H, Kaas E, Kjær KH, Korsgaard NJ, Larsen NK, Linderson H, Lyså A, Möller P, Olsen J, Willerslev E (2011). A 10,000-year record of Arctic Ocean sea-ice variability–view from the beach. Science 333, 747-750.

Georgiadis E, Giraudeau J, Martinez P, Lajeunesse P, St-Onge G, Schmidt S, Massé G (2018). Deglacial to postglacial history of Nares Strait, Northwest Greenland: a marine perspective from Kane Basin. Climate of the Past 14, 1991-2010.

Georgiadis E, Giraudeau J, Jennings A, Limoges A, Jackson R, Ribeiro S, Massé G (2020). Local and regional controls on Holocene sea ice dynamics and oceanography in Nares Strait, Northwest Greenland. Marine Geology 422, 106115.

Gibb O, Steinhauer S, Fréchette B, de Vernal A, Hillaire-Marcel C (2015). Diachronous evolution of sea surface conditions in the Labrador Sea and Baffin Bay since the last deglaciation. Holocene 25 (12), 1882-1897.

Giraudeau J, Grelaud M, Solignac S, Andrews JT, Moros M, Jansen E (2010). Millennial-scale variability in Atlantic water advection to the Nordic Seas derived from Holocene coccolith concentration records. Quaternary Science Reviews 29, 1276-1287.

Giraudeau J, Georgiadis E, Caron M, Martinez P, Massé G, Saint-Onge G, Billy I, Lebleu P, Ther O. (2020) A high-resolution elemental record of post-glacial lithic sedimentation in Upernavik Trough, western Greenland: History of ice-sheet dynamics and ocean circulation changes over the last 9100 years. Global and Planetary Change 191, 103217. https://doi.org/10.1016/j.gloplacha.2020.103217

Gosselin M, Legendre L, Therriault JC, Demers S, Rochet M (1986). Physical control of the horizontal patchiness of sea-ice microalgae. Mar. Ecol. Progr. Ser. 29, 289-298.

Grove JM (2004). Little Ice Ages: Ancient and Modern. Routledge, New York.

Hansen KE, Massé, G, Giraudeau, J, Pearce, C, Seidenkrantz, M-S (2020) Reconstruction of Holocene oceanographic conditions in Northeastern Baffin Bay. Climate of the Past 16, 1075-1095.

Hillaire-Marcel C, de Vernal A (2008). Stable isotope clue to episodic sea ice formation in the glacial North Atlantic. Earth Planetary Science Letter 268, 143-150.

Heikkilä M, Pospelova V, Hochheim KP, Kuzyk ZZA, Stern GA, Barber DG, Macdonald RW (2014). Surface sediment dinoflagellate cysts from the Hudson Bay system and their relation to freshwater and nutrient cycling. Marine Micropaleontology 106, 79-109.

Holland DM, Thomas RH, De Young B, Ribergaard MH, Lyberth B (2008). Acceleration of Jakobshavn Isbræ triggered by warm subsurface ocean waters. Nature Geoscience 1 (10), 659-664.

Hopwood MJ, Carroll D, Browning TJ, Meire L, Mortensen J, Krisch S, Achterberg EP (2018). Non-linear response of summertime marine productivity to increased meltwater discharge around Greenland. Nature Communications 9, 3256.

Howe JA, Austin WEN, Forwick M, Paetzel M (2010). Dinoflagellate cysts as proxies for palaeoceanographic conditions in Arctic fjords (eds) Fjord Systems and Archives. Geological Society, London, Special Publications, 344, 61–74. DOI: 10.1144/SP344.6

Jennings AE, Knudsen KL, Hald M, Hansen CV, Andrews JT (2002). A mid-Holocene shift in Arctic sea-ice variability on the East Greenland shelf. Holocene 12, 49-58.

Jennings AE, Andrews J, Wilson L (2011). Holocene environmental evolution of the SE Greenland shelf north and south of the Denmark strait: Irminger and east Greenland current interactions. Quaternary Sciences Reviews 30, 980-998.

Jennings AE, Walton ME, Cofaigh CÓ, Kilfeather A, Andrews JT, Ortiz JD, de Vernal A, Dowdeswell JA (2014). Paleoenvironments during Younger Dryas-Early Holocene retreat of the

Greenland Ice Sheet from outer Disko Trough, central west Greenland. Journal of Quaternary Science 29(1), 27-40.

Jennings AE, Andrews JT, Oliver B, Walczak M, Mix A (2019). Retreat of the Smith Sound Ice Stream in the Early Holocene. Boreas 48, 825-840.

Kemp AES, Pike J, Pearce RB, Lange CB (2000). The "Fall dump" — a new perspective on the role of a "shade flora" in the annual cycle of diatom production and export flux. Deep-Sea Res II 47, 2129–2154.

Kemp AES, Pearce RB, Grigorov I, Rance J, Lange CB, Quilty P (2006). Production of giant marine diatoms and their export at oceanic frontal zone: Implications for Si and C flux from stratified oceans. Global biogeochemical cycles 20, GB4S04.

Knudsen KL, Stabell B, Seidenkrantz MS, Eiríksson J, Blake W (2008). Deglacial and Holocene conditions in northernmost Baffin Bay: sediments, foraminifera, diatoms and stable isotopes. Boreas 37, 346-376.

Koch CW, Cooper LW, Lalande C, Brown TA, Frey KE, Grebmeier JM (2020). Seasonal and latitudinal variations in sea ice algae deposition in the Northern Bering and Chukchi Sea determined by algal biomarkers. PLoS ONE 15 (4): e0231178.

Krembs C, Eicken H, Deming J.W. (2011). Exopolymer alteration of physical properties of sea ice and implications for ice habitability and biogeochemistry in a warmer Arctic. Proceedings of the National Academy of Sciences, 108(9), 3653–3658.

Krawczyk DW Witkowski A, Moros M, Lloyd J, Kuijpers A, Kierzek (2010). Late-Holocene diatom inferred reconstruction of temperature variations of the West Greenland Current from Disko Bugt, central West Greenland. Holocene 20 (5), 659-666.

Krawczyk DW, Witkowski A, Lloyd J, Moros M, Harff J, Kuijpers A (2013). Late-Holocene diatom derived seasonal variability in hydrological conditions off Disko Bay, West Greenland. Quaternary Science Reviews 67, 93-104.

Krawczyk DW, Witkowski A, Waniek J, Wroniecki M, Harff J (2014). Description of diatoms from the Southwest to West Greenland coastal and open marine waters. Polar Biology 37, 1589-1606.

Krawczyk DW, Witkowski A, Moros M, Lloyd JM, Høyer, Miettinen A (2017). Quantitative reconstruction of Holocene sea ice and sea surface temperature off West Greenland from the first regional diatom data set. Paleoceanography 32, 18-40.

Lafond A, Leblanc K, Quéguiner B, Moriceau B, Leynaert A, Cornet V, Legras J, Ras J, Parenteau M, Garcia N, Babin M, Tremblay J-E (2019). Late spring bloom development of pelagic diatoms in Baffin Bay. Elementa: Science of the Anthropocene 7, 44.

Lalande C, Nöthig E-M, Fortier L (2019). Algal export in the Arctic Ocean in times of global warming. Geophysical Research Letter, 46.https://doi.org/10.1029/2019GL083167

Laskar J, Robutel P, Joutel F, Gastineau M, Correia ACM, Levrard B (2004). A long-term numerical solution for the insolation quantities of the Earth. Astronomy and Astrophysics 428: 261-285.

Lasher GE, Axford Y, McFarlin JM, Kelly MA, Osterberg EC, Berkelhammer MB (2017). Holocene temperatures and isotopes of precipitation in Northwest Greenland recorded in lacustrine organic materials. Quaternary Science Reviews 170, 45-55.

Lecavalier BS, Fisher DA, Milne GA, Vinther BM, Tarasov L, Huybrechts P, Lacelle D, Main B, Zheng J, Bourgeois J, Dyke AS (2017). High Arctic Holocene temperature record from the Agassiz ice cap and Greenland ice sheet evolution. PNAS 114 (23), 5952-5957.

Lehmann N, Kienast M, Granger J, Bourbonnais A, Altabet MA, Tremblay JÉ (2019). Remote western Arctic nutrients fuel remineralization in deep Baffin Bay. Global Biogeochemical Cycles 33, 649-667.

Levac E, de Vernal A, Blake WJ (2001). Sea-surface conditions in northernmost Baffin Bay during the Holocene: Palynological evidence. Journal of Quaternary Science 16, 353-363.

Limoges A, Massé G, Weckström K, Poulin M, Ellegaard M, Heikkilä M, Geilfus N-X, Sejr MK, Rysgaard S and Ribeiro S (2018a). Spring Succession and Vertical Export of Diatoms and IP_{25} in a Seasonally Ice-Covered High Arctic Fjord. Frontiers in Earth Sciences 6, 226. doi: 10.3389/feart.2018.00226

Limoges A, Ribeiro S, Weckström K, Heikkilä M, Zamelczyk K, Andersen TJ, Tallberg P, Massé G, Rysgaard S, Nørgaard-Pedersen N, Seidenkrantz M-S (2018b). Linking the modern distribution of biogenic proxies in high Arctic Greenland shelf sediments to sea ice, primary production, and Arctic-Atlantic inflow. Journal of Geophysical Research: Biogeosciences, 123.

Litchman E, and Klausmeier C A (2008). Trait-based community ecology of phytoplankton. Annual Review of Ecology Evolution and Systematics 39, 615–639. doi: 10.1146/annurev.ecolsys.39.110707.173549

Lovejoy C, Legendre L, Martineau M-J, Bâcle J, von Quillfeldt CH (2002). Distribution of phytoplankton and other protists in the North Water. Deep-Sea Res II 49:5027–5047.

Lloyd JM, Moros M, Perner K, Telford RJ, Kuijpers A, Jansen E, McCarthy D (2011). A 100 yr record of ocean temperature control on the stability of Jakobshavn Isbrae, West Greenland. Geology 39, 867-870.

Luostarinen T, Ribeiro S, Weckström K, Sejr M, Meire L, Tallberg P, Heikkilä M (2020). An annual cycle of diatom succession in two contrasting Greenlandic fjords: from simple sea-ice indicators to varied seasonal strategists. Marine Micropaleontology. https://doi.org/10.1016/j.marmicro.2020.101873

Manabe S and Wetherald RT (1975). The effects of doubling the CO_2 concentration on the climate of a general circulation model. Journal of Atmospheric Science 32, 3–15.

McQuoid MR, Hobson LA (1996). Diatom resting stages. Journal of Phycology 32, 889-902.

Meyers PA (1994). Preservation of elemental and isotopic source identification of sedimentary organic matter. Chemical Geology 114 (3-4), 289-302.

Moffa-Sánchez P, Hall IR (2017). North Atlantic variability and its link to European climate over the last 3000 years. Nature Communications 8, 1726.

Møller HS, Jensen KG, Keuijpers A, Aagaard-Sørensen S, Seidenkrantz M-S, Endler R, Mikkelsen N (2006). Late Holocene environmental and climatic changes in Ameralik Fjord, southwest Greenland – evidence from the sedimentary record. Holocene 16, 685-695.

Morley A, Rosenthal Y, deMenocal P (2014). Ocean-atmosphere climate shift during the mid-to-late Holocene transition. Earth and Planetary Science Letters 388, 13-26.

Moros M, Jansen E, Oppo DW, Giraudeau J, Kuijpers A (2012). Reconstruction of the late-Holocene changes in the Sub-Arctic Front position at the Reykjanes Ridge, north Atlantic. The Holocene 22(8), 877-886.

Moros M, Lloyd J, Perner K, Krawczyk D, Blanz T, de Vernal A, Ouellet-Bernier M-M, Kuijpers A, Jennings A, Witkowski A, Schneider R, Jansen E (2016). Surface and sub-surface multi-proxy

reconstruction of middle to late Holocene palaeoceanographic changes in Disko Bugt, West Greenland. Quaternary Science Reviews 132, 146-160.

Mudie PT, Rochon A, Levac E (2005). Decadal-scale sea-ice changes in the Canadian Arctic and their impacts on humans during the past 4,000 years. Environmental Archaeology 10, 113-126.

Mundy CJ, Gosselin M, Ehn J, Gratton Y, Rossnagel A, Barber DG, Martin J, Tremblay JÉ, Palmer M, Arrigo KR, Darnis G, Fortier L, Else B, Papakyriakou T (2009). Contribution of under-ice primary production to an ice-edge upwelling phytoplankton bloom in the Canadian Beaufort Sea. Geophysical Research Letters 36, L17601. doi:10.1029/2009GL038837

Myers PG, Kulan N, Ribergaard MH (2007). Irminger Water variability in the West Greenland Current. Geophysical Research Letters 34, L17601.

Noren AJ, Bierman PR, Steig EJ, Lini A, Southon J (2002). Millennial-scale storminess variability in the northeastern United States during the Holocene epoch. Nature 419, 821-824.

Odebrecht C and Djurfeldt L (1996). The role of nearshore mixing on phytoplankton size structure of Cape Santa Marta Grande, southern Brazil (Spring 1989). Archive of Fishery and Marine Research 43(3), 217–230.

Oksman M, Juggins S, Miettinen A, Witkowski A, Weckström K (2019). The biogeography and ecology of common diatom species in the northern North Atlantic, and their implications for paleoceanographic reconstructions. Marine Micropaleontology 148, 1-28.

Olsen J, Anderson NJ, Knudsen MF (2012). Variability of the North Atlantic Oscillation over the past 5,200 years. Nature Geoscience 5, 808-812.

Ogi M and Wallace JM (2007). Summer minimum Arctic sea ice extent and the associated summer atmospheric circulation. Geophysical Research Letters 34, L12705.

Oppo DW, McManus JF, Cullen JL (2003). Deepwater variability in the Holocene epoch. Nature 422, 277-278.

Ouellet-Bernier M-M, de Vernal A, Hillaire-Marcel C, Moros M (2014). Paleoceanographic changes in the Disko Bugt area, west Greenland, during the Holocene. Holocene 24, 1573-1583.

Pearce C, Weckström K, Sha L, Miettinen A, Seidenkrantz M-S (2014). The Holocene marine diatom flora of Eastern Newfoundland bays. Diatom Research 29 (4), 441-454.

Perner K, Moros, M, Jennings A, Lloyd JM, Knudsen KL (2012). Holocene paleoceanographic evolution off West Greenland. The Holocene 23 (3), 374-387.

Perner K, Moros M, Snowball I, Lloyd JM, Kuijpers A, Richter T (2013). Establishment of modern circulation pattern at c. 6000 cal a BP in Disko Bugt, central West Greenland: opening of the Vaigat Strait. Journal of Quaternary Science 28(5), 480-489

Poulin M, Cardinal A, Legendre L (1983). Réponse d'une communauté de diatomées de glace à un gradient de salinité (baie d'Hudson). Marine Biol. 76, 191-202.

Poulin M, Underwood GJC, Michel C (2014). Sub-ice colonial *Melosira arctica* in Arctic first year-ice. Diatom Research, 26(2) 213-221.

Post E and Forchhammer MC (2002). Synchronization of animal population dynamics by large-scale climate. Nature 420, 168-171.

Ramsey CB (2008). Deposition models for chronological records. Quaternary Science Reviews 27 (1–2), 42-60.

Rasmussen TL, Thomsen E, Troelstra SR, Kuijpers A, Prins MA (2002). Millennial-scale glacial variability versus Holocene stability: changes in planktic and benthic foraminifera faunas and ocean circulation in the North Atlantic during the last 60 000 years. Marine Micropaleontology 47, 143–176.

Rau GH, Takahashi T, Desmarais DJ, Repeta DJ, Martin JH (1992). The relationship between d13C or organic matter and CO_2[aq] in ocean surface-water–Data from a JGOFS site in the northeast Atlantic Ocean and a model. Geochimica et Cosmochimica Acta 56(3), 1413-1419.

Reimer PJ et al. (2013). IntCal13 and Marine13 radiocarbon age calibration curves 0-50,000 years cal BP. Radiocarbon 55(4), 1869-1887.

Ribeiro S, Sejr MK, Limoges A, Heikkilä M, Andersen TJ, Tallberg P, Weckström K, Husum K, Forwick M, Dalsgaard T, Massé G, Seidenkrantz M-S, Rysgaard S (2017). Sea ice and primary production proxies in surface sediments from a High Arctic Greenland fjord: spatial distribution and implications for palaeoenvironmental studies. Ambio 46 (Suppl. 1) S106-S118.

Rigor IG, Wallace JM, Colony RL (2002). Response of sea ice to the Arctic Oscillation. Journal of Climate 15, 2648-2663.

Robinson RS, Kienast M, Albuquerque AL, Altabet M, Contreras S,De Pol Holz R,Dubois N, Francois R, Galbraith E, Hsu T-C, Ivanochko T, Jaccard S, Kao S-J, Kiefer T, Kienast S, Lehmann M, Martinez P, McCarthy M, Möbius J,Pedersen T, Quan TM, Ryabenko E, Schmittner A, Schneider R,Schneider-Mor A, Shigemitsu M, Sinclair D, Somes C, Studer A, Thunell R, Yang J-Y (2012). A review of nitrogen isotopic alteration in marine sediments. Paleoceanography 27, PA4203, doi:10.1029/2012PA002321

Rodwell MJ, Rowell DP, Folland CK (1999). Oceanic forcing of the wintertime North Atlantic Oscillation and European climate. Nature 398, 320-323.

Rowland S, Allard W, Belt S, Massé G, Rober J-M, Blackburn S, Frampton D, Revill AT, Volkman JK (2001). Factors influencing the distributions of polyunsaturated terpenoids in the diatom, *Rhizosolenia setigera*. Phytochemistry 58(5), 717-728.

Saini J, Stein R, Fahl K, Weiser J, Hebbeln D, Hillaire-Marcel C, de Vernal A (2020). Holocene variability in sea ice and primary productivity in the northeastern Baffin Bay. Arktos 168.

Sarafanov A (2009). On the effect of the North Atlantic Oscillation on temperature and salinity of the subpolar North Atlantic intermediate and deep waters. ICES Journal of Marine Science 66 (7), 1448–1454. https://doi.org/10.1093/icesjms/fsp094

Schweinsberg AD, Briner JP, Miller GH, Bennike O, Thomas EK (2017). Local glaciation in West Greenland linked to North Atlantic Ocean circulation during the Holocene. Geology 45 (3), 195-198.

Seidenkrantz M-S, Aagaard-Sørensen S, Sulsbrück H, Kuijpers A, Jensen KG, Kunzendorf H (2007). Hydrography and climate of the last 4400 years in a SW Greenland fjord: implications for Labrador Sea palaeoceanography. Holocene 17, 387-401.

Serreze M., Barrett AP, Slater AG, Woodgate RA, Aagaard K, Lammers RB, Steele M, Moritz R, Meredith M, Lee CM (2006). The large-scale freshwater cycle of the Arctic. J. Geophys. Res. 111. https://doi.org/10.1029/2005JC003424

Serreze M, Barrett A, Stroeve J, Kindig D, Holland M (2009). The emergence of surface-based Arctic amplification. Cryosphere 3, 11–19.

Serreze M and Stroeve J (2015). Arctic sea ice trends, variability and implications for seasonal ice forecasting. Philosophical transactions Royal Society A 373, 20140159.

Serreze MC, Stroeve J, Barrett AP, Boisvert LN (2016). Summer atmospheric circulation anomalies over the Arctic Ocean and their influences on September sea ice extent: A cautionary tale. J. Geophys. Res. Atmospheres 121, 11,463-11,485. https://doi.org/10.1002/2016JD025161

Sha L, Jiang H, Knudsen KL (2011). Diatom evidence of climatic change in Holsteinsborg Dyb, west of Greenland, during the last 1200 years. The Holocene 22(3), 347-358.

Smik L, Belt ST, Lieser J, Armand LK, Leventer A (2016). Variations in algal lipid distributions in seasonally sea-ice covered surface waters from East Antarctica: further insights for biomarker-based paleo sea-ice reconstructions. Organic Geochemistry 95, 71-80.

Solignac S, de Vernal A, Hillaire-Marcel C (2004). Holocene sea-surface conditions in the North Atlantic—contrasted trends and regimes in the western and eastern sectors (Labrador Sea vs. Iceland Basin). Quaternary Science Reviews 23, 319–334.

Staines-Urías F, Kuijpers A, Korte C (2013). Evolution of subpolar North Atlantic surface circulation since the early Holocene inferred from planktic foraminifera faunal and stable isotope records. Quaternary Science Reviews 76, 66-81.

Steele M, Morison J, Ermold W, Rigor I, Ortmeyer M, Shimada K (2004). Circulation of summer Pacific halocline water in the Arctic Ocean. J. Geophys. Res. 109 C02027. doi:10.1029/2003JC002009.

St-Onge M-P, St-Onge G (2014). Environmental changes in Baffin Bay during the Holocene based on the physical and magnetic properties of sediment cores. Journal of Quaternary Science 29 (1) 41-56.

Straneo F (2006). Heat and Freshwater Transport through the Central Labrador Sea. Journal of Physical Oceanography 36, 606-628.

Talley LD, Pickard GL, Emery WJ, Swift JH (2011). Chapter S15 - Climate and the Oceans, Editor(s): Lynne D. Talley, George L. Pickard, William J. Emery, James H. Swift, Descriptive Physical Oceanography (Sixth Edition), Academic Press, p.1-36, ISBN 9780750645522, https://doi.org/10.1016/B978-0-7506-4552-2.10027-7.

Tedesco I, Vichi M, Scoccimarro E (2019). Sea-ice algal phenology in a warmer Arctic. Science Advances 5: eaav4830.

Thomas EK, Briner JP, Ryan-Henry JJ, Huang Y (2016). A major increase in winter snowfall during the middle Holocene on western Greenland caused by reduced sea ice in Baffin Bay and the Labrador Sea. Geophysical Research Letters 43, 5302-5308.

Thompson DWJ and Wallace JM (1998). The Arctic Oscillation signature in the wintertime geopotential height and temperature fields. Geophysical Research Letters 25 (9), 1297-1300.

Thompson DWJ and Wallace JM (2001). Regional climate impacts of the Northern Hemisphere Annular Mode. Science 293 (5527), 85-89.

Tréguer P, Bowler C, Moriceau B, Dutkiewicz S, Gehlen M, Aumont O, Bittner L, Dugdale R, Finkel Z, Ludicone D, Jahn O, Guidi L, Lasbleiz M, Leblanc K, Levy M, Pondaven P (2018). Influence of diatom diversity on the ocean biological pump. Nature Geoscience 11, 27-37.

Tremblay, JÉ, Robert, D., Varela, DE, Lovejoy C, Darnis G, Nelson RJ, Sastri AR (2012). Current state and trends in Canadian Arctic marine ecosystems: I. Primary production. Climatic Change (2012) 115: 161. https://doi.org/10.1007/s10584-012-0496-3

Tremblay JÉ, Anderson LG, Matrai P, Coupel P, Bélanger S, Michel C, Reigstad M (2015). Global and regional drivers of nutrient supply, primary production and CO_2 drawdown in the changing Arctic Ocean. Progress in Oceanography 139, 171–196.

Van Nieuwenhove N, Baumann A, Matthiessen J, Bonnet S, de Vernal A (2016). Sea surface conditions in the southern Nordic Seas during the Holocene based on dinoflagellate cyst assemblages. The Holocene, 1-14.

Van Nieuwenhove N, Pearce C, Knudsen MF, Røy H, Seidenkrantz MS (2018). Meltwater and seasonality influence on Subpolar Gyre circulation during the Holocene. Palaeogeography, Palaeoclimatology, Palaeoecology 502, 104-118.

Vinther BM, Buchardt SL, Clausen HB, Dahl-Jensen D, Johnsen SJ, Fisher DA, Koerner RM, Raynaud D, Lipenkov V, Andersen KK, Blunier T, Rasmussen SO, Steffensen JP, Svensson AM (2009) Holocene thinning of the Greenland ice sheet. Nature 461, 385-388

Von Quillfeldt CH (2001). Identification of some easily confused diatom species in Arctic spring blooms. Botanica Marina 44, 375-389.

Von Quillfeldt CH, Ambrose WG, Clough LM (2003). High number of diatom species in first-year ice from the Chukchi Sea. Polar Biology 26, 806-818.

Von Quillfeldt CH (2004). The diatom *Fragilariopsis cylindrus* and its potential as an indicator species for cold water rather than for sea ice. Vie Milieu 54, 137-143.

Vinther BL, Buchardt SL, Clausen HB, Dahl-Jensen D, Johnsen SJ, Fisher DA, Koerner RM, Raynaud D, Lipenkov V, Andersen KK, Blunier T, Rasmussen SO, Steffensen JP, Svensson AM (2009). Holocene thinning of the Greenland ice sheet. Nature 461, 385-388.

Wallace JM (2000). North Atlantic Oscillation/annular mode: Two paradigms–one phenomenon. Q.J.R. Meteorol. Soc. 126, 791-805.

Wanner H, Beer J, Bütikofer J, Crowley TJ, Cubasch U, Flückiger J, Goosse H, Grosjean M, Joos F, Kaplan JO, Küttel M, Müller SM, Prentice C, Solomina O, Stocker TF, Tarasov P, Wagner M, Widmann M (2008). Mid- to Late Holocene climate change: an overview. Quaternary Science Reviews 27, 1791-1828.

Weckström K, Massé G, Collins LG, Hanhijärvi S, Bouloubassi I, Sicre M-A, Seidenkrantz M-S, Schmidt S, Andersen TJ, Andersen ML, Hill B, Kuijpers A (2013). Evaluation of the sea ice proxy IP25 against observational and diatom proxy data in the SW Labrador Sea. Quaternary Science Reviews 79, 53-62.

Weckström K, Redmond Roche B, Miettinen A, Krawczyk D, Limoges A, Juggins S, Ribeiro S, Heikkilä M (2020). Improving the paleoceanographic proxy tool kit – on the biogeography and ecology of the sea ice-associated species *Fragilariopsis oceanica*, *Fragilariopsis reginae-jahniae* and *Fossula arctica* in the northern North Atlantic. Marine Micropaleontology 157, 101860.

Weston K, Fernand L, Mills DK, Delahunty R, Brown J (2005). Primary production in the deep chlorophyll maximum of the central North Sea. Journal of plankton research 27, 909-922.

Williams KM (1986). Recent Arctic marine diatom assemblages from bottom sediments in Baffin Bay and Davis Strait. Marine Micropaleontology 10, 327-341.

Williams, KM (1990). Late Quaternary paleoceanography of the western Baffin Bay region: evidence from fossil diatoms. Canadian Journal of Earth Sciences 27, 1487–1494.

Young NE and Briner JP (2015). Holocene evolution of the western Greenland Ice Sheet: Assessing geophysical ice-sheet models with geological reconstructions of ice-margin change. Quaternary Science Reviews 114, 1-17.

Zweng MM, Münchow A (2006). Warming and freshening of Baffin Bay, 1916-2003. Journal of Geophysical Research 111, C07016

TABLES

Table 1. Radiocarbon dates for core AMD14-204.

Sample depth midpoint (cm)	Lab. ID	Material	^{14}C age (yr BP)	Calibrated age range (cal yr. BP), 1s	Modelled median age (cal. yr BP)	δ^{3}C
4.5	ETH-92277	Mixed benthic foraminifera	705±50	167-276	213	4.94
70.5	ETH-92279	Mixed benthic foraminifera	1795±50	1175-1270	1216	4.22
70.5	ETH-92278	Mixed planktonic foraminifera	1710±50	1032-1175	1101	6.12
170	SacA 46004	Mixed benthic & planktonic foraminifera	3555±35	3139-3260	3192	5,7
250.5	BETA 467785	Mixed benthic & planktonic foraminifera	4300±30	4133-4254	4199	0.3
310.5	ETH-92281	Mixed benthic foraminifera	4950±60	4860-4992	4941	3.06
310.5	ETH-92280	Mixed planktonic foraminifera	4940±70	4930-5188	5043	5.7

410.5	ETH-92283	Mixed benthic foraminifera	5805±60	5905-6005	5959	1.68
410.5	ETH-92282	Mixed planktonic foraminifera	5825±60	5984-6155	6063	3.41
501.5	BETA 488641	Mixed benthic foraminifera	6400±30	6656-6751	6707	-1.8
580.5	ETH-92285	Mixed benthic foraminifera	7155±70	7430-7531	7483	2.95
580.5	ETH-92284	Mixed planktonic foraminifera	7005±60	7298-7417	7356	2.38
610	SacA 46005	Mixed benthic foraminifera & ostracods	7445±50	7712-7822	7766	-6,9
700.5	ETH-92286	Mixed benthic foraminifera	8270±389	8639-8885	8755	-
737.5	ETH-92287	Mixed benthic foraminifera	8489±154	9017-9302	9162	-

FIGURE CAPTIONS

Figure 1. A) Greenland Ice sheet and historical median sea-ice extent (1981-2010) for the months of February (dashed dark blue line), July (dashed light blue line) and September (dashed orange line). Also shown is the July average extent of the North Water polynya (NOW) for the same period. **B)** Simplified representation of the main surface ocean currents discussed here: The West Greenland Current (WGC) forms by the convergence of the East Greenland Current (EGC) and Irminger Current (IC), a branch of the North Atlantic Current (NAC), as they round the southern tip of Greenland. **C)** Location of core AMD14-204 (yellow circle) studied here, and other cores from northern Baffin Bay and Kane Basin discussed in the text. Abbreviations: BB: Baffin Bay, BG: Beaufort Gyre, JS: Jones Sound, LS: Lancaster Sound, NOW: North Water polynya, SPG: Subpolar Gyre, and TPD: Transpolar drift.

Figure 2. A) Age-depth model for core AMD14-204. The light blue envelope represents the modelled 1 sigma range, and the blue line marks the modelled median age. The light-shaded areas for each radiocarbon date indicate the probability distribution prior to modelling, whereas the darker areas indicate the posterior probability distribution. The color code for the dates indicates the material used: Blue: mixed benthic foraminifera, red: mixed planktonic foraminifera, grey: mixed planktonic and benthic foraminifera, green: mixed ostracods, planktonic and benthic foraminifera. **B)** Sedimentation rate (cm kyr^{-1}).

Figure 3. Temporal changes in selected biogenic proxies for the past ca. 9000 cal. years before present (BP). From top to bottom: **A)** fluxes of the HBI III source species *Rhizosolenia hebetata* f. *semispina* (valves unit surface^{-1} yr^{-1}), **B)** HBI III fluxes (ng unit surface^{-1} yr^{-1}; filled area; left Y-axis), median value (dashed line; left Y-axis) and absolute concentrations normalized to TOC (ng/gTOC; line; right Y-axis), **C)** IP_{25} fluxes (ng unit surface^{-1} yr^{-1}; filled area; left Y-axis), median value (dashed line; left Y-axis) and absolute concentrations normalized to TOC (ng/gTOC; full line; right Y-axis), **D)** nitrogen isotopic signature (‰), **E)** carbon isotopic signature (‰)**,** and **F)** total organic carbon (TOC) fluxes (g unit surface^{-1} yr^{-1}; filled area; left axis) and content (wt%; full line; right Y-axis).

Figure 4. Carbon isotopic values ($\delta^{13}C$, ‰) against TOC:TN ratios of bulk organic matter. The color code indicates the age of the samples. The arrows indicate that ice particulate OM is more enriched in ^{13}C compared to pelagic particulate OM values due to limited atmospheric CO_2-exchange in the sea ice (e.g., Rau et al. 1992), and land-derived OM yields higher TOC:TN ratios (20 to 100; Meyers, 1994) than aquatic OM (typically between 4 and 10, Meyers, 1994). Our data indicate a pelagic-dominant signature, with varying mixing ratios between pelagic, sympagic and terrestrial organic matter. In general, the elemental and isotopic signature of the organic matter shows that samples younger than 4.5 kyrs BP (indicated by the grey box), and especially between 3 and 1.2 kyrs BP, contain higher ratios of ice-derived organic material.

Figure 5. Relative abundances (%) of the main diatom taxa (excluding *Chaetoceros* resting spores), absolute concentrations (valves g^{-1}) of diatom valves (filled area) and *Chaetoceros* spp. (resting spores; line), and total diatom fluxes (valves unit surface^{-1} yr^{-1}; includes both diatom valves and *Chaetoceros* spores).

Figure 6. Summary figure showing primary production and sea-ice dynamics in relation with the AO index and Holocene climate development. From top to bottom: **A)** summer and spring insolation (W/m^2) at 73°N (Laskar *et al*. 2004); **B)** oxygen isotopic ratios (‰) at Camp Century (Vinther *et al.* 2009); **C)** abundance of Kara Sea ice-rafted Fe oxide grains in the Beaufort gyre (Darby *et al.* 2012); **D)** relative contribution of the Atlantic water indicator foraminiferal group from core AMD14-204 (%, Hansen *et al.* 2020); **E)** relative contribution of the warm water indicator dinocyst taxon *Operculodinium centrocarpum* from core AMD14-204 (%, Caron *et al.* 2019); **F)** IP_{25} fluxes (ng unit surface^{-1} yr^{-1}; this study); **G)** HBI III fluxes (ng unit surface^{-1} yr^{-1}; this study); **H)** relative contribution of the "summer subsurface" assemblage (%) (this study), **I)** relative contribution of the "marginal ice zone" assemblage (%) (this study), **J)** relative contribution of the "drift-ice/pack-ice" assemblage (%), (this study) and **K)** total diatom fluxes (valves unit surface^{-1} yr^{-1}, dark green includes *Chaetoceros* spores and light green excludes *Chaetoceros* spores (this study). The grey areas indicate intervals of persistent positive AO phases (Darby *et al.* 2012; Funder *et al.* 2011). Abbreviations: LIA: Little Ice Age, MCA: Medieval Climate Anomaly, DA: Dark Age, RWP: Roman Warm Period, and IA: Iron Age.

Figure 7. Simplified schematic representation of surface circulation under persistent low and high AO polarity index. The areas coloured in red and blue reflect the milder and colder atmospheric winter temperatures during negative and positive AO phases, respectively. **A)** During AO(-), a strong Beaufort gyre promotes the formation of multiyear sea ice and is linked to generally reduced export of freshwater and ice from the Arctic Ocean via Fram Strait (Rigor *et al.* 2002). The transpolar drift stream follows the Lomonosov Ridge (Steele *et al.* 2004; Talley *et al.* 2011). The East Greenland Current, an extension of the transpolar drift, is relatively weaker. Multiyear ice and weaker winds may facilitate the formation of ice bridges in Nares Strait, restricting export fluxes through this gateway (Georgiadis *et al.* 2020). In the North Atlantic, a relatively contracted subpolar gyre facilitates the entrainment of warm and salty Irminger waters into the WGC (e.g., Sarafanov 2009; Morley *et al.* 2014). **B)** During AO(+) a weaker Beaufort gyre is associated with thinner Arctic Ocean sea ice, especially in the eastern sector (Rigor *et al.* 2002), which enhances sea-ice mobility and favors the export of solid and liquid freshwater via the main Arctic gateways. The transpolar drift stream flows nearly directly from the Bering Strait to the northern side of Greenland (Steele *et al.* 2004). This translates into increased EGC strength. Thinner Arctic sea ice and strong winds may contribute to weaken the Nares Strait ice bridges (Georgiadis *et al.* 2020), promoting freshwater and drift-ice exports through this gateway. Export across the Canadian Arctic Archipelago channels is mainly in the form of liquid freshwater (Serreze *et al.* 2006). Atmospheric temperatures over Labrador, Greenland and the western subpolar North Atlantic decrease (Talley *et al.* 2011). AO(+) is associated with strong westerlies, cold sea-surface temperatures in the Labrador Sea and subpolar gyre, and expansion of the subpolar gyre, with consequent decreased northwestward entrainment of Atlantic waters, which are confined to the easternmost part of the North Atlantic (e.g., Sarafanov 2009; Morley *et al.* 2014). Abbreviations: WGC: West Greenland Current, EGC: East Greenland current, IC: Irminger Current, SPG: Subpolar Gyre, BG: Beaufort Gyre, and TPD: Transpolar drift.

PLATES

Plate 1. Micrographs of selected diatom taxa observed in the sediment core AMD14-204: 1) *Thalassiosira antarctic*a var. *borealis* (resting spore primary valve), 2) *Thalassiosira antarctic*a var. *borealis* (resting spore secondary valve), 3) *Actinocyclus curvatulus*, 4) *Thalassiosira nordenskioeldii,* 5) *Melosira arctica,* 6) *Bacterosira bathyomphala,* 7) *Fragilariopsis reginae-jahniae,* 8) *Fragilariopsis oceanica,* 9) *Fossula arctica,* 10) Fragment of *Thalassiothrix longissima,* 11) *Fragilariopsis cylindrus,* 12) Fragment of *Rhizosolenia hebetata* f. *semispina, 13)* Fragment of *Rhizosolenia hebetata* var. *hebetata.* Scale bar: 10 µm.

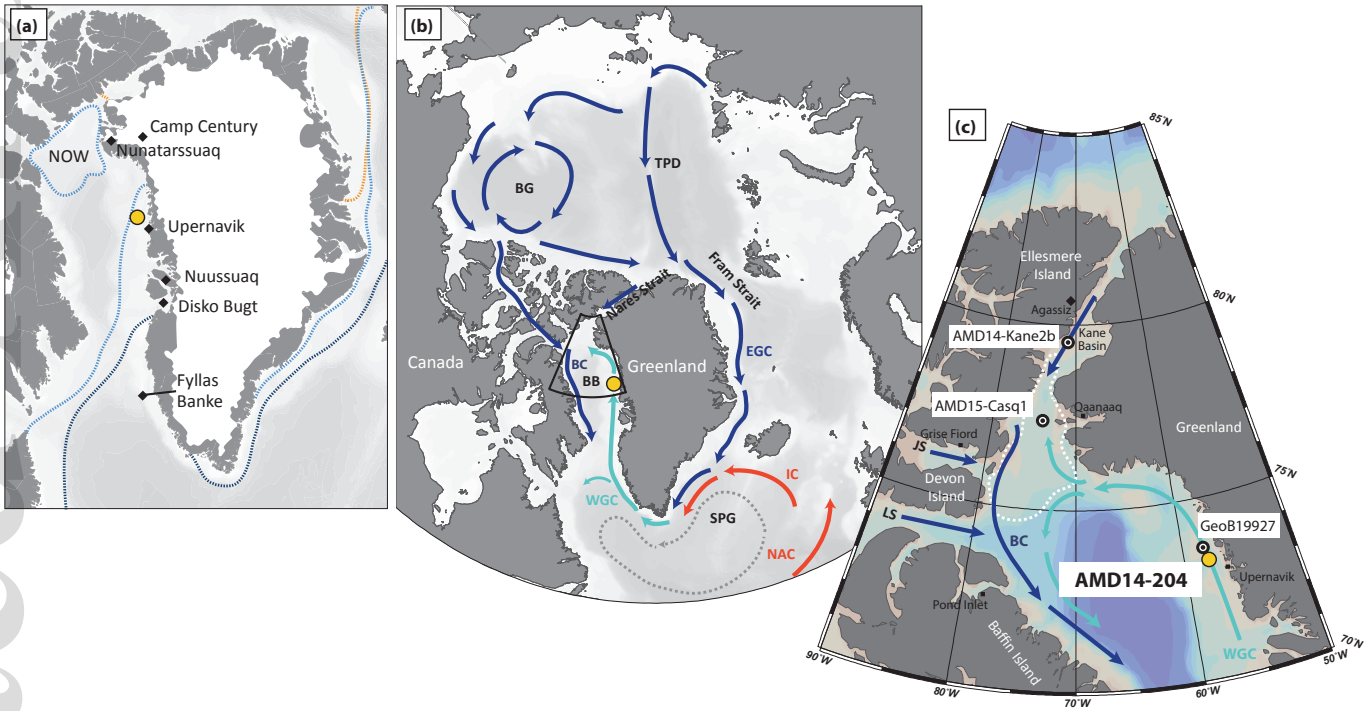

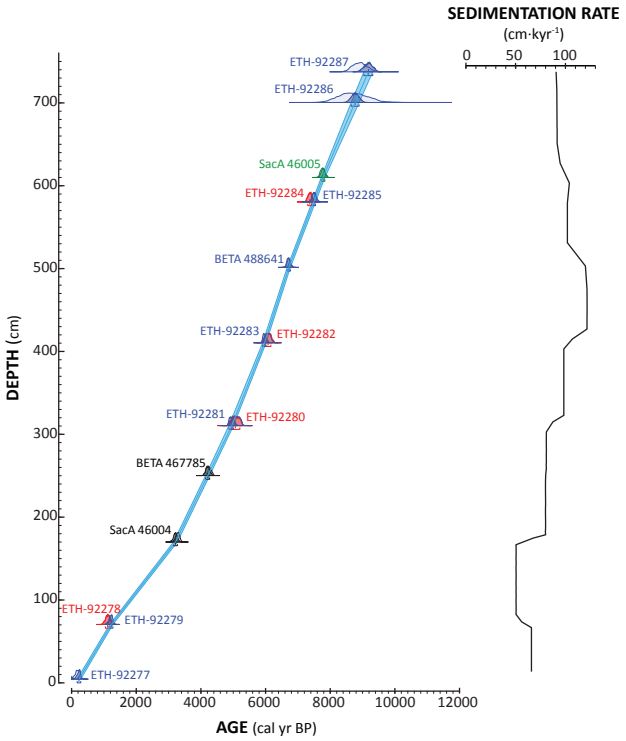

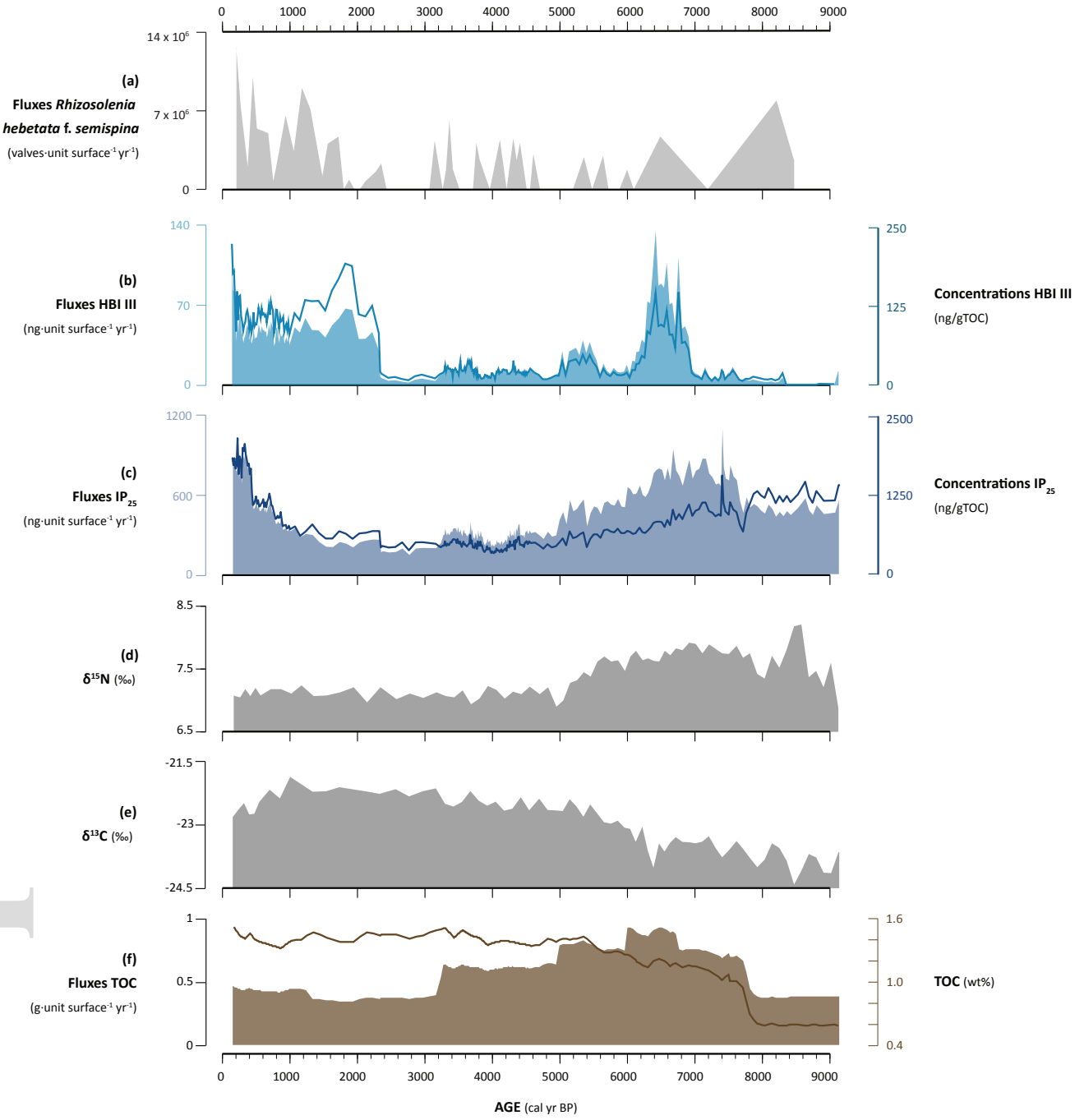

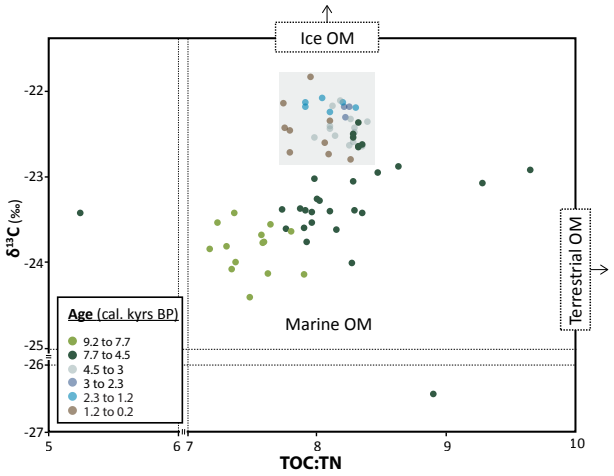

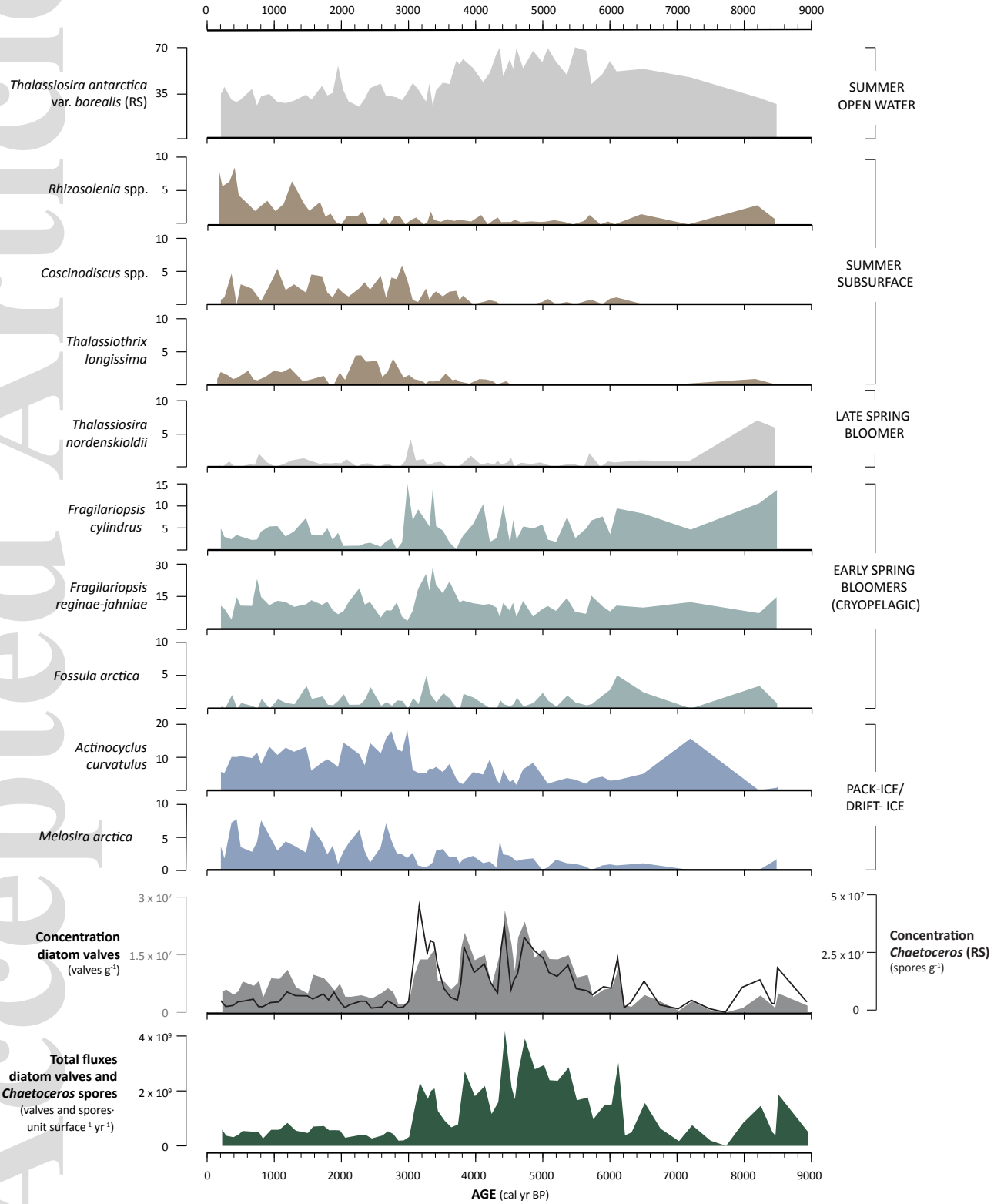

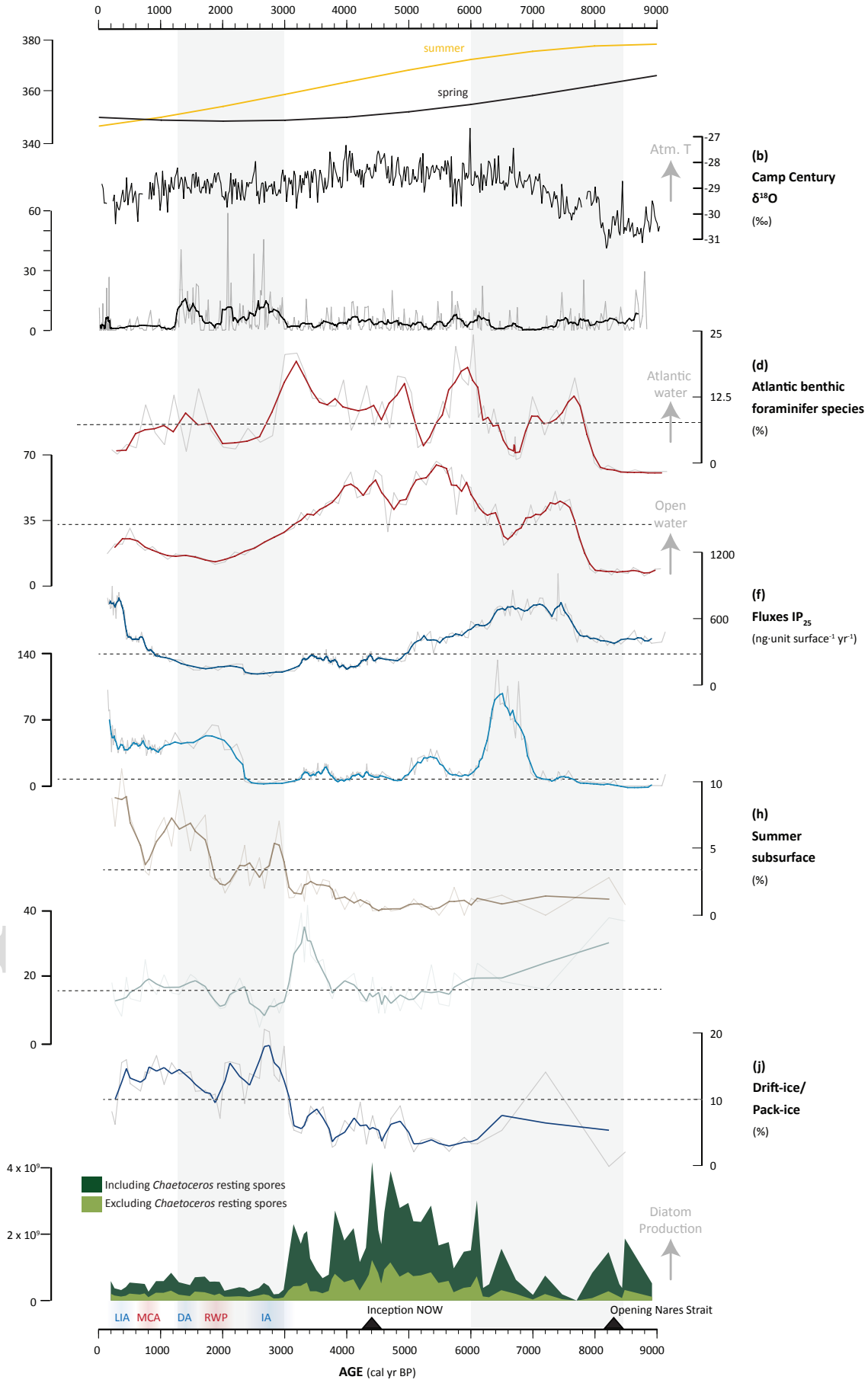

Dominant AO(–) phase
(6 to 3 kyrs BP, and 1.2 to 0.2 kyrs BP)

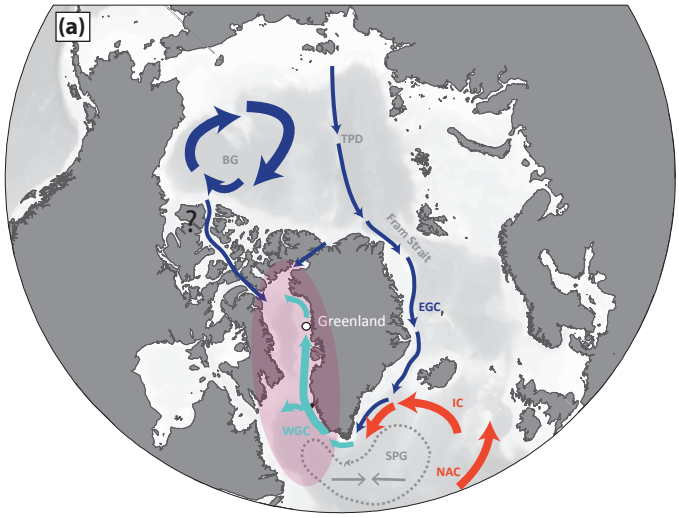

Dominant AO(+) phase
(3 to 1.2 kyrs BP)

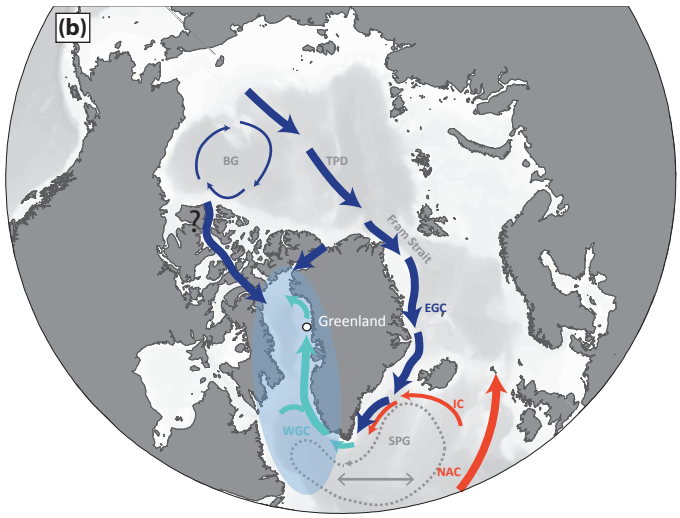

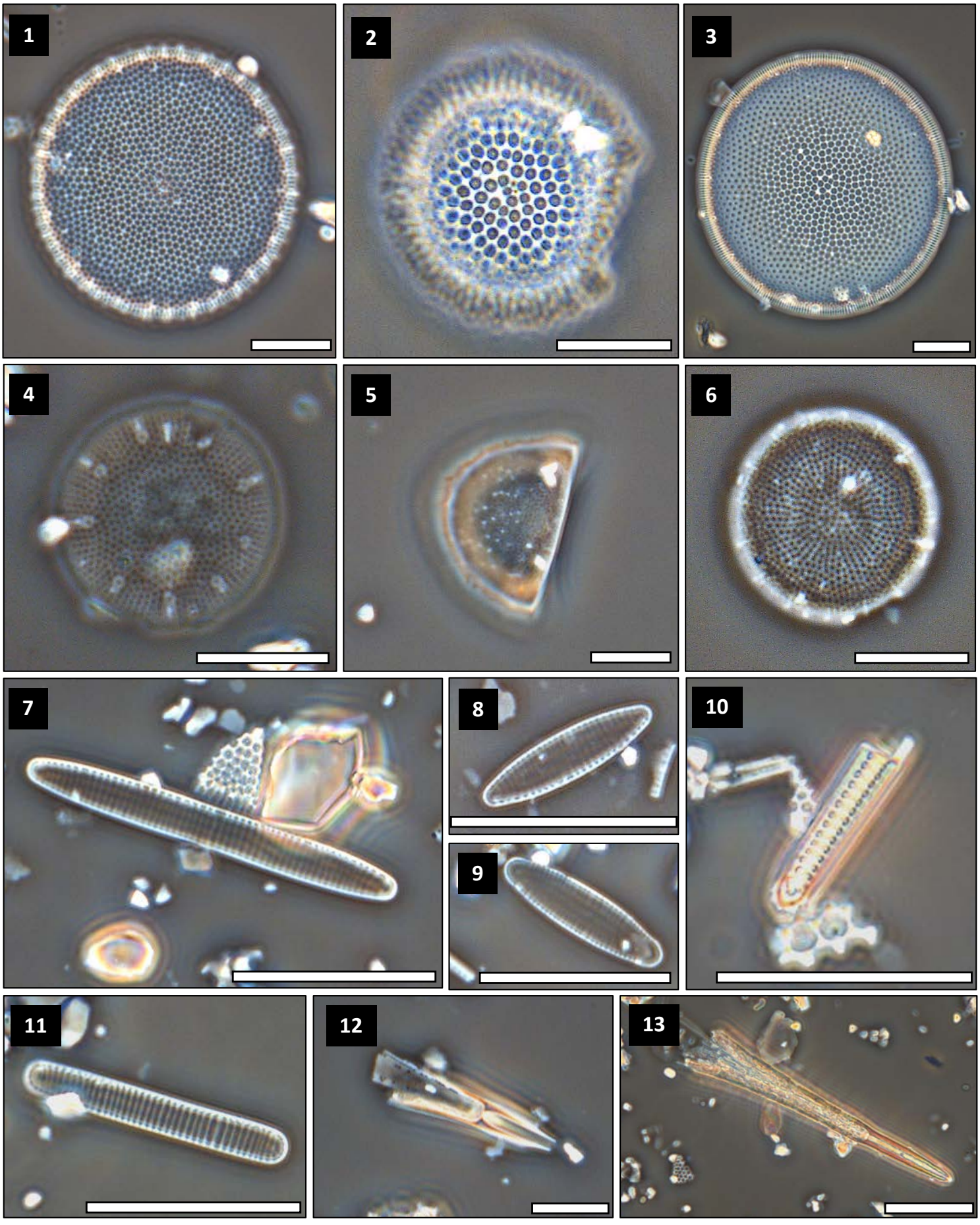
1
2
3
4
5
6
7
8
9
10
11
12
13